On the scattering of elastic waves from a non-axisymmetric defect in a coated pipe

Wenbo Duan [a,*], Ray Kirby [b], Peter Mudge [c]

[a] Brunel Innovation Centre, Brunel University, Uxbridge, Middlesex UB8 3PH, UK
[b] School of Engineering and Design, Brunel University, Uxbridge, Middlesex UB8 3PH, UK
[c] NDT Technology Group, TWI Ltd, Cambridge CB21 6AL, UK

ARTICLE INFO

ABSTRACT

Viscoelastic coatings are often used to protect pipelines in the oil and gas industry. However, over time defects and areas of corrosion often form in these pipelines and so it is desirable to monitor the structural integrity of these coated pipes using techniques similar to those used on uncoated pipelines. A common approach is to use ultrasonic guided waves that work on the pulse-echo principle; however, the energy in the guided waves can be heavily attenuated by the coating and so significantly reduce the effective range of these techniques. Accordingly, it is desirable to develop a better understanding of how these waves propagate in coated pipes with a view to optimising test methodologies, and so this article uses a hybrid SAFE-finite element approach to model scattering from non-axisymmetric defects in coated pipes. Predictions are generated in the time and frequency domain and it is shown that the longitudinal family of modes is likely to have a longer range in coated pipes when compared to torsional modes. Moreover, it is observed that the energy velocity of modes in a coated pipe is very similar to the group velocity of equivalent modes in uncoated pipes. It is also observed that the coating does not induce any additional mode conversion over and above that seen for an uncoated pipe when an incident wave is scattered by a defect. Accordingly, it is shown that when studying coated pipes one need account only for the attenuation imparted by the coating so that one may normally neglect the effect of coating on modal dispersion and scattering.

1. Introduction

Viscoelastic materials are often used as coatings on the outer surface of pipelines in order to protect the pipe from external damage and corrosion. However, over time it is possible for these coatings to degrade and for regions of corrosion or other defects to form within the pipe substrate. Accordingly, it is desirable to monitor the integrity of the pipe and a fast and efficient way to do this is through the use of non-destructive testing (NDT) techniques such as long range ultrasonic testing (LRUT) [1,2]. The application of LRUT to coated pipes involves sending a guided wave along the pipe wall, but this technique is less successful for coated pipes because the viscoelastic coating attenuates the ultrasonic wave as it travels along the pipe wall. This has the effect of significantly reducing the range over which LRUT can be successfully used in the location of defects such as corrosion. This presents a significant problem because LRUT is an important tool for interrogating pipelines and the use of viscoelastic coatings is relatively widespread. It is desirable, therefore, to try and develop a better

understanding of the way in which a coating attenuates an ultrasonic wave, as well as how it affects the scattering of waves from defects. One approach to achieving a better understanding is through the development of theoretical models, however there are very few articles in the literature that use theoretical models to analyse scattering from defects in a pipeline coated with a viscoelastic material. Accordingly, this article utilises a three dimensional model that is suitable for analysing scattering from defects of arbitrary shape in a pipe of arbitrary length coated with a viscoelastic material. In doing so this model moves away from relying on dispersion curves in order to analyse a scattering problem that is more representative of problems found in the field.

A typical pipeline consists of a long and uniform pipe in which the defect, or region of corrosion, forms only over a short section of the pipe. LRUT works by sending an incident pulse down the pipe and then recording the reflected pulse scattered by the defect. The energy contained within the incident and reflected pulse travels as a series of eigenmodes and so one must be careful to excite the appropriate mode, or modes, as well as to retain some understanding of the characteristics of each mode when interpreting the returning pulse, and here a knowledge of group velocity is

important when distinguishing modal content. Therefore, understanding the properties of the pipe eigenmodes is very important in the practical application of LRUT and so a common starting point for a theoretical analysis of coated pipes is to find the pipe eigenmodes, or dispersion curves as they are known. This approach is illustrated for coated pipes by Barshinger and Rose [3], who applied a global transfer matrix method to compute the phase and attenuation of axisymmetric longitudinal modes. The global matrix method derives an analytic expression for the governing dispersion relation and so numerical routines are necessary to find the complex roots of this equation. Root finding in the complex plane is often difficult and time consuming, especially at higher frequencies [3] and so it is advantageous to use alternative methods. Accordingly, numerical techniques are becoming increasingly popular and one of the most reliable and efficient methods for obtaining the eigenmodes of a uniform structure is the semi analytic finite element (SAFE) method. This approach substitutes an analytic expression for the displacement in the axial direction into Navier's governing equation and then uses the finite element method to solve the resulting two dimensional eigenequation. Thus, one only needs to mesh the cross section of the structure, and the SAFE method may be applied to structures with an arbitrary cross-section provided they are uniform in the axial direction. A rigorous introduction to the SAFE method is provided by Bartoli et al. [4], who proceed to apply the method to a waveguide of arbitrary cross-section, as well as a viscoelastic plate; for other examples of the application of the SAFE method see [5–9]. Mu and Rose [10] also applied the SAFE method to pipes with a viscoelastic coating, and by using an analytic expansion for the circumferential direction they were able to further reduce the problem to one dimension. Moreover, through the use of an orthogonality relation for the pipe eigenmodes, Mu and Rose were able to sort values for phase velocity and attenuation for a large number of propagating eigenmodes. Further applications of the SAFE method to problems involving energy dissipation include the work of Castaings and Lowe [11], who calculate the eigenmodes for a waveguide of arbitrary cross-section that is surrounded by an absorbing region, and Marzani et al. [12] who examined multi-layered structures and computed the energy velocity for the eigenmodes, which is generally more appropriate than group velocity for structures in which material damping is present [13]. Thus, the SAFE method has now been shown to deliver a reliable and efficient means for finding the eigenmodes in a waveguide containing material damping and so this method is well suited to studying coated pipes. Accordingly, this article will make use of the SAFE method to calculate eigenmodes for uniform regions of a coated pipe and in the section that follows the SAFE method is applied to a two dimensional problem.

The SAFE method is very useful for finding the eigenmodes in an infinitely long structure, however the eigenexpansion assumes that the structure is uniform. If one is also to model the scattering from a defect then this adds considerable additional complexity, especially if one also wishes to study a non-axisymmetric defect. Modelling difficulties are caused by the non-uniformities in the structure and whilst it is possible simply to numerically discretise an entire pipe this likely to require extremely high numbers of degrees of freedom even for modest pipe lengths. Moreover, discretising the entire pipe obviously cannot be achieved if the pipe is infinite, and so this approach normally requires some form of non-reflecting boundary in order to close the problem for an equivalent finite length of pipe. An example of the finite element method was presented by Hua and Rose [14], who studied a short length of coated pipe. Hua and Rose used commercial software and studied the attenuation of guided waves in a uniform pipe where there is no additional mode conversion at the end of the pipe, however this method will quickly generate excessive degrees of freedom if one

moves to more representative geometries. Predoi et al. [15] used an absorbing boundary layer method to study scattering from a defect in a two dimensional viscoelastic plate and it is clear that extension to three dimensions is likely to become computationally expensive. It is also possible to reduce computational expenditure by introducing higher order finite elements and Żak [16] demonstrates the application of the spectral element method to wave propagation in a plate. The spectral finite element is now well developed for structural health monitoring and the increase in computational efficiency that this provides means that it is now capable of being applied to relatively large structures [17], however one must still mesh the entire structure and this is not always the most attractive option, especially for structures such as pipelines that are long and slender. Moreover, structures such as pipelines also have a relatively simple geometry and it is possible to take advantage of this when developing a numerical model. This is achieved by using alternative methods for modelling wave propagation in the long uniform sections found in pipe installations, or similar guided wave applications. For example, Galán and Abascal [18] used a hybrid boundary element-finite element approach to study scattering from a defect in a plate coated with a viscoelastic material; this approach then reduces the degrees of freedom required in the uniform section through the use of a boundary element discretisation. An alternative approach that is potentially even more efficient is to use a modal expansion for the uniform section of pipe and to couple this to a numerical discretisation that surrounds only the defect being studied. This will radically reduce the number of degrees of freedom required when compared to a full discretisation and in principle it can be used for any length of pipe without incurring additional computational costs. A relevant example of this approach for uncoated pipes is the method of Zhou et al. [19], who used the wave finite element method to solve the eigenequation in the uniform section, and then coupled this to a finite element discretisation surrounding the defect. Recently Benmeddour et al. [20] used a hybrid SAFE-finite element (FE) method to analyse elastic wave propagation in a solid cylinder, and Duan and Kirby [21] used a similar method to analyse elastic wave propagation in an uncoated pipe. The article by Duan and Kirby contains a more detailed discussion about these and other alternative numerical approaches and so these will not be discussed further here. However, it is noticeable that in the literature the only application of a hybrid SAFE-FE approach to coated pipes was that reported by Kirby et al. [22,23]. The models developed by Kirby et al. were used primarily to deduce the bulk shear and longitudinal properties of the viscoelastic coating, and to do this it was necessary only to study the axisymmetric problem. Therefore, Kirby et al. restricted their analysis to either torsional [22] or longitudinal [23] modes, and so these approaches are not suitable for studying the more general problem of scattering from non-axisymmetric defects.

The aim of this article is to analyse scattering from non-axisymmetric defects in coated pipes using the hybrid SAFE-FE method. Relevant examples of the application of this method to elastic wave propagation in circular geometries include the articles by Benmeddour et al. [20], and Duan and Kirby [21]. Note that Benmeddour et al. use a variational formulation, whilst Duan and Kirby use a weighted residual formulation to derive the final system of equations. Thus, in Section 2 a weighted residual formulation is adopted for the three dimensional problem. In Section 3 predictions generated using a three dimensional model are validated against two dimensional predictions and measurements. In Sections 4 and 5 predictions are generated that quantify scattering from a non-axisymmetric defect representative of corrosion in a coated pipe, and here predictions are presented in the frequency and time domain. Parametric studies are also undertaken and

conclusions drawn regarding the influence of the coating and on the choice of excitation when undertaking LRUT in coated pipes.

2. Theory

The theory reported in this section is based on the hybrid SAFE-FE method described by Duan and Kirby [21]. However, the analysis of a coated pipe requires the addition of an extra layer when compared to the analysis reported by Duan and Kirby [21]. Accordingly, when adding an additional layer it is convenient to use a normalisation procedure that is different to that used by Duan and Kirby, as this facilitates the writing of the final governing equations in a computationally efficient way. The governing equation for wave propagation in an elastic or viscoelastic medium is Navier's equation, which is written as

$$\left(\lambda_{p,c} + \mu_{p,c}\right)\nabla\left(\nabla \cdot \mathbf{u}'_{p,c}\right) + \mu_{p,c}\nabla^2 \mathbf{u}'_{p,c} = \rho_{p,c}\frac{\partial^2 \mathbf{u}'_{p,c}}{\partial t^2}, \tag{1}$$

where λ and μ are the Lamé constants, $\mathbf{u}'$ is the displacement vector, ρ is density and t is time. A time dependence of $e^{i\omega t}$ is assumed throughout this article, where ω is the radian frequency and $i = \sqrt{-1}$. The subscripts p and c denote pipe and coating respectively. Navier's equation is applied here to an infinite pipe coated with a viscoelastic material, see Fig. 1, with the coating applied to the outer surface. The pipe also contains a single defect that is arbitrary in shape and which penetrates both the coating and the pipe substrate. The boundary condition for this problem is assumed to be traction free on the outer surface of the coating and the inner surface of the pipe. On the interface between the pipe and the coating, the displacement and traction forces are equal. A hybrid SAFE-finite element approach is adopted so that a numerical discretisation is used for a region surrounding the defect (this is Ω_2 in Fig. 1), and for those uniform sections abutting this region a modal expansion is adopted (regions Ω_1 and Ω_3). Thus, for the uniform sections the SAFE method is applied to find the pipe eigenmodes and this is discussed in the following section; a full finite element discretisation of Ω_2 is then discussed in Section 2.2.

2.1. SAFE method for a coated pipe

The displacements u'_{1q} in region Ω_1 of the pipe are expanded over the pipe eigenmodes to give
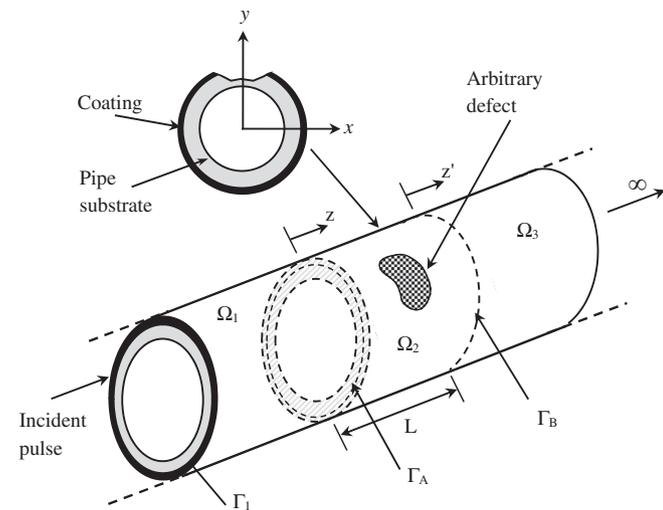
Fig. 1. Geometry of coated pipe containing arbitrary defect.

$$u'_{1q}(x,y,z) = \sum_{n=0}^{\infty} u^n_{1q}(x,y)e^{-ik\gamma^n z}, \tag{2}$$

where the subscript $q = x, y$ or z, and $u_{1q}(x,y)$ are the eigenvectors in region Ω_1, where $k = \omega/c_{Tp}$ so that γ is a (coupled) dimensionless wavenumber. In addition, c_{Tp} and c_{Lp} are the shear (torsional) and compressional (longitudinal) bulk wave velocities in the pipe substrate, respectively. Further, c_{Tc} and c_{Lc} are the shear (torsional) and compressional (longitudinal) bulk wave velocities in the viscoelastic coating, respectively. The finite element analysis proceeds by discretising the displacements of any mode n over the pipe cross-section to give

$$u_{1q}(x,y) = \sum_{j=1}^{p_{1q}} N_{qj}(x,y)u_{1qj} = \mathbf{N}_q \mathbf{u}_{1q}, \tag{3}$$

where N_{qj} is a global trial (or shape) function, u_{1qj} is the value of u_{1q} at node j, and p_{1q} is the number of nodes (or degrees of freedom) for the displacements in direction q. In addition, $\mathbf{N}_q$ and $\mathbf{u}_{1q}$ are row and column vectors of length p_{1q}, respectively, and it is convenient to choose $\mathbf{N}_x = \mathbf{N}_y = \mathbf{N}_z$ so that one only needs to generate one finite element mesh. The displacement can be further divided as $\mathbf{u}_{1q} = [\mathbf{u}_{1qp}\mathbf{u}_{1qc}]^T$, where $\mathbf{u}_{1qp}$ and $\mathbf{u}_{1qc}$ denote nodal displacements in the pipe and in the coating, respectively. This also facilitates the application of continuity of displacement and traction forces over the interface between the pipe and the coating, and after applying these continuity conditions and enforcing zero traction on the internal surface of the pipe and the outer edge of the coating [21], the substitution of Eq. (3) into Eq. (1) yields the following eigenequation:

$$\mathbf{P}\mathbf{u}_1 = \gamma\mathbf{S}\mathbf{u}_{1,} \tag{4}$$

where $\mathbf{u}_1 = [\mathbf{u}_{1x} \quad \mathbf{u}_{1y} \quad \mathbf{u}_{1z} \quad \gamma\mathbf{u}_{1x} \quad \gamma\mathbf{u}_{1y} \quad \gamma\mathbf{u}_{1z}]^T$. It is convenient to split up matrices $\mathbf{P}$ and $\mathbf{S}$ so that

$$\mathbf{P}\mathbf{u}_1 = \mathbf{P}_p\mathbf{u}_{1p} + \mathbf{P}_c\mathbf{u}_{1c} \tag{5}$$

$$\mathbf{S}\mathbf{u}_1 = \mathbf{S}_p\mathbf{u}_{1p} + \mathbf{S}_c\mathbf{u}_{1c} \tag{6}$$

where $\mathbf{u}_{1p,c} = [\mathbf{u}_{1xp,c} \quad \mathbf{u}_{1yp,c} \quad \mathbf{u}_{1zp,c} \quad \gamma\mathbf{u}_{1xp,c} \quad \gamma\mathbf{u}_{1yp,c} \quad \gamma\mathbf{u}_{1zp,c}]^T$, and the constituents of matrices $\mathbf{P}_{p,c}$ and $\mathbf{S}_{p,c}$ are given in Appendix A. Eq. (4) is a sparse symmetric eigenequation that is solved for the eigenmodes in the coated pipe. The method for solving this equation and for sorting the eigenmodes that are obtained is described by Duan and Kirby [21]. This solution delivers $p_1 = p_3 = p_{1x} + p_{1y} + p_{1z}$ eigenmodes.

Modal attenuation and energy velocity are two of the most important factors to be considered when examining wave propagation in a coated pipe. Attenuation quantifies the reduction in amplitude of the wave, whereas the energy velocity determines the velocity of the "centre of gravity" of a wave as it propagates along the pipe wall [24]. For attenuative waves in coated pipes, energy velocity more accurately represents the velocity of a wave package, although of course the energy velocity reduces to the group velocity for an uncoated pipe. The attenuation (Δ) is defined in the usual way:

$$\Delta = -20\Im(k) \times \log_{10}(e). \tag{7}$$

The energy velocity is defined as the ratio of the average power flow to the average stored energy per unit length of the waveguide [24] to give

$$V_e = \frac{2Re\left\{\sum_{\tau=p,c}\int_{\Gamma_{A\tau}}\left[-\sigma_{1zq-}\cdot u^*_{1q-}\right]d\Gamma_{A\tau}\right\}}{Re\left\{\sum_{\tau=p,c}\int_{\Gamma_{A\tau}}\left[\rho_{\tau}u_{1q-}\cdot u^*_{1q-} + \sigma_{1ql-}:\varepsilon^*_{1ql-}\right]d\Gamma_{A\tau}\right\}}. \tag{8}$$

Here, the superscript $*$ indicates the complex conjugate, and q and l take on values of x, y and z, with the summation convention applying to repeated indices of q and l. In addition, u_{1q-}, σ_{1ql-} and ε_{1ql-} are the incident displacements, stress and strain tensors in region Ω_1. The first term in the denominator represents the kinetic energy density and the second term the strain energy density.

2.2. A hybrid SAFE-FE approach for a coated pipe

A three dimensional finite element discretisation is used for the non-uniform section of the pipe, Ω_2, which is assumed to contain a defect of arbitrary shape, see Fig. 1. The displacements $u'_{2q}(x, y, z)$ in Ω_2 are discretised to give

$$u'_{2q}(x,y,z) = \sum_{j=1}^{p_{2q}} W_{qj}(x,y,z)u_{2qj} = \mathbf{W}_q \mathbf{u}_{2q}, \tag{9}$$

where W_{qj} is a global shape function, and u_{2qj} is the value of u'_{2q} at node j, and p_{2q} is the number of nodes in the q direction. For convenience when matching with the inlet and outlet regions, we choose $\mathbf{W}_x = \mathbf{W}_y = \mathbf{W}_z = \mathbf{W}$ so that the weak forms of Eq. (1) yields

$$\int_{\Omega_2} \left\{ \left[(\lambda_{p,c} + \mu_{p,c}) \frac{\partial \mathbf{W}^T}{\partial x} \frac{\partial \mathbf{W}}{\partial x} + \mu_{p,c} \nabla \mathbf{W}^T \nabla \mathbf{W} - \rho \omega^2 \mathbf{W}^T \mathbf{W} \right] \mathbf{u}_{2xp,c} \right.$$
$$+ \left[\lambda_{p,c} \frac{\partial \mathbf{W}^T}{\partial x} \frac{\partial \mathbf{W}}{\partial y} + \mu_{p,c} \frac{\partial \mathbf{W}^T}{\partial y} \frac{\partial \mathbf{W}}{\partial x} \right] \mathbf{u}_{2yp,c}$$
$$\left. + \left[\lambda_{p,c} \frac{\partial \mathbf{W}^T}{\partial x} \frac{\partial \mathbf{W}}{\partial z} + \mu_{p,c} \frac{\partial \mathbf{W}^T}{\partial z} \frac{\partial \mathbf{W}}{\partial x} \right] \mathbf{u}_{2zp,c} \right\} d\Omega_2 = \int_{\Gamma_2} \mathbf{W}^T h_{2xp,c} d\Gamma_2, \tag{10a}$$

$$\int_{\Omega_2} \left\{ \left[\lambda_{p,c} \frac{\partial \mathbf{W}^T}{\partial y} \frac{\partial \mathbf{W}}{\partial x} + \mu_{p,c} \frac{\partial \mathbf{W}^T}{\partial x} \frac{\partial \mathbf{W}}{\partial y} \right] \mathbf{u}_{2xp,c} + \left[(\lambda_{p,c} + \mu_{p,c}) \frac{\partial \mathbf{W}^T}{\partial y} \frac{\partial \mathbf{W}}{\partial y} \right. \right.$$
$$\left. + \mu_{p,c} \nabla \mathbf{W}^T \nabla \mathbf{W} - \rho \omega^2 \mathbf{W}^T \mathbf{W} \right] \mathbf{u}_{2yp,c}$$
$$\left. + \left[\lambda_{p,c} \frac{\partial \mathbf{W}^T}{\partial y} \frac{\partial \mathbf{W}}{\partial z} + \mu_{p,c} \frac{\partial \mathbf{W}^T}{\partial z} \frac{\partial \mathbf{W}}{\partial y} \right] \mathbf{u}_{2zp,c} \right\} d\Omega_2 = \int_{\Gamma_2} \mathbf{W}^T h_{2yp,c} d\Gamma_2, \tag{10b}$$

$$\int_{\Omega_2} \left\{ \left[\lambda_{p,c} \frac{\partial \mathbf{W}^T}{\partial z} \frac{\partial \mathbf{W}}{\partial x} + \mu_{p,c} \frac{\partial \mathbf{W}^T}{\partial x} \frac{\partial \mathbf{W}}{\partial z} \right] \mathbf{u}_{2xp,c} + \left[\lambda_{p,c} \frac{\partial \mathbf{W}^T}{\partial z} \frac{\partial \mathbf{W}}{\partial y} \right. \right.$$
$$\left. + \mu_{p,c} \frac{\partial \mathbf{W}^T}{\partial y} \frac{\partial \mathbf{W}}{\partial z} \right] \mathbf{u}_{2yp,c} + \left[(\lambda_{p,c} + \mu_{p,c}) \frac{\partial \mathbf{W}^T}{\partial z} \frac{\partial \mathbf{W}}{\partial z} + \mu_{p,c} \nabla \mathbf{W}^T \nabla \mathbf{W} \right.$$
$$\left. \left. - \rho \omega^2 \mathbf{W}^T \mathbf{W} \right] \mathbf{u}_{2zp,c} \right\} d\Omega_2 = \int_{\Gamma_2} \mathbf{W}^T h_{2zp,c} d\Gamma_2. \tag{10c}$$

Here, the notation for the pipe substrate and coating regions follows the conventions used in the previous section. Similarly, it is necessary also to enforce continuity of displacement and traction force between the coating and the pipe, as well as enforce zero traction force over the outer surface of Ω_2, apart from the surfaces Γ_A and Γ_B, so that

$$h_{2qp,c} = \sigma_{2qlp,c} n_l = 0, \tag{11}$$

where the indices q and l take on values of x, y and z, and the summation convention applies to repeated indices of l only. In Eq. (11), σ_{ql} denotes the Cauchy stress tensor and n_l is the unit outward normal vector to the surface of the pipe so that

$$h_{xp,c} = \lambda_{p,c} \left(\frac{\partial u'_{2xp,c}}{\partial x} + \frac{\partial u'_{2yp,c}}{\partial y} + \frac{\partial u'_{2zp,c}}{\partial z} \right) n_x + 2\mu_{p,c} \frac{\partial u'_{2xp,c}}{\partial x} n_x$$
$$+ \mu_{p,c} \left(\frac{\partial u'_{2xp,c}}{\partial y} + \frac{\partial u'_{2yp,c}}{\partial x} \right) n_y$$
$$+ \mu_{p,c} \left(\frac{\partial u'_{2xp,c}}{\partial z} + \frac{\partial u'_{2zp,c}}{\partial x} \right) n_z, \tag{12a}$$

$$h_{yp,c} = \mu_{p,c} \left(\frac{\partial u'_{2yp,c}}{\partial x} + \frac{\partial u'_{2xp,c}}{\partial y} \right) n_x$$
$$+ \lambda_{p,c} \left(\frac{\partial u'_{2xp,c}}{\partial x} + \frac{\partial u'_{2yp,c}}{\partial y} + \frac{\partial u'_{2zp,c}}{\partial z} \right) n_y + 2\mu_{p,c} \frac{\partial u'_{2yp,c}}{\partial y} n_y$$
$$+ \mu_{p,c} \left(\frac{\partial u'_{2yp,c}}{\partial z} + \frac{\partial u'_{2zp,c}}{\partial y} \right) n_z, \tag{12b}$$

$$h_{zp,c} = \mu_{p,c} \left(\frac{\partial u'_{2zp,c}}{\partial x} + \frac{\partial u'_{2xp,c}}{\partial z} \right) n_x + \mu_{p,c} \left(\frac{\partial u'_{2zp,c}}{\partial y} + \frac{\partial u'_{2yp,c}}{\partial z} \right) n_y$$
$$+ \lambda_{p,c} \left(\frac{\partial u'_{2xp,c}}{\partial x} + \frac{\partial u'_{2yp,c}}{\partial y} + \frac{\partial u'_{2zp,c}}{\partial z} \right) n_z + 2\mu_{p,c} \frac{\partial u'_{2zp,c}}{\partial z} n_z. \tag{12c}$$

Continuity of displacement and traction force between the coating and the pipe is implemented naturally in region 2 once the region is discretised appropriately.

The displacements in regions Ω_1 and Ω_3 are written as modal expansions using solutions from the previous section, so that

$$u'_{1q}(x,y,z) = \sum_{n=0}^{m_1} A^n u^n_{1q+}(x,y)e^{-ik_\gamma^n z} + \sum_{n=0}^{m_1} B^n u^n_{1q-}(x,y)e^{ik_\gamma^n z}, \tag{13}$$

and

$$u'_{3q}(x,y,z') = \sum_{n=0}^{m_1} C^n u^n_{1q+}(x,y)e^{-ik_\gamma^n z'}. \tag{14}$$

Here, A^n, B^n and C^n are modal amplitudes, and u^n_{1q+} and u^n_{1q-} are eigenvectors for the incident and reflected waves, respectively. The number of modes used in the analysis for regions Ω_1 and Ω_3 is m_1, where $m_1 \leqslant p_1$. It is assumed that the pipe extends to infinity in region Ω_3 so that no reflected waves are present in this region. In addition, Eq. (13) allows for a general incident sound field, although in the analysis that follows this will be restricted either to torsional $T(0,1)$ or longitudinal $L(0,2)$ excitation as this best reflects experimental practice.

The problem is solved by enforcing continuity of displacement and traction forces in the axial direction over the interface between the uniform pipe sections and the central finite element based solution. Each continuity condition is weighted using the method described by Duan and Kirby in [21] and this delivers a final system equation of the form:

$$\begin{bmatrix} -\mathbf{G}_{11-} & \mathbf{G}_{21}^T & \mathbf{G}_{31}^T & \mathbf{G}_{41-}^T & \mathbf{0} \\ \mathbf{G}_{21} & \mathbf{G}_{22} & \mathbf{G}_{32}^T & \mathbf{G}_{42}^T & \mathbf{G}_{25} \\ \mathbf{G}_{31} & \mathbf{G}_{32} & \mathbf{G}_{33} & \mathbf{G}_{43}^T & \mathbf{G}_{35} \\ \mathbf{G}_{41-} & \mathbf{G}_{42} & \mathbf{G}_{43} & \mathbf{G}_{44} & \mathbf{G}_{45} \\ \mathbf{0} & \mathbf{G}_{25}^T & \mathbf{G}_{35}^T & \mathbf{G}_{45}^T & \mathbf{G}_{55} \end{bmatrix} \begin{Bmatrix} \mathbf{B} \\ \mathbf{u}_{2x} \\ \mathbf{u}_{2y} \\ \mathbf{u}_{2z} \\ \mathbf{C} \end{Bmatrix} = \begin{Bmatrix} \mathbf{G}_{11+}\mathbf{A} \\ \rho c_s^2 [\mathbf{Q}_{1x+} - \mathbf{Q}_{1zx+}]\mathbf{A} \\ \rho c_s^2 [\mathbf{Q}_{1y+} - \mathbf{Q}_{1zy+}]\mathbf{A} \\ -\mathbf{G}_{41+}\mathbf{A} \\ \mathbf{0} \end{Bmatrix}. \tag{15}$$

Eq. (15) is a set of n_t $(= 2m_1 + p_2)$ linear equations, where p_2 is the number of degrees of freedom in region Ω_2 and m_1 is the number of modes in regions Ω_1 and Ω_3 respectively. The vectors $\mathbf{A}$, $\mathbf{B}$ and $\mathbf{C}$ hold the modal amplitudes A^n, B^n and C^n respectively, and the other matrices are given in Appendix B. The modal amplitudes in Ω_1 and Ω_3, and the displacements in region Ω_2 are therefore found on the solution of Eq. (15). The displacements in Ω_1 and Ω_3 are then obtained from Eqs. (13) and (14).

The modal amplitudes defined in Eqs. (13) and (14) are independent of location in region Ω_1. However, the displacement amplitude is dependent on location because the coating attenuates energy. Therefore, in order to study wave scattering from a defect without the influence of location, the reflection coefficient is defined here using a plane that is immediately adjacent to the left hand side of the defect. Thus, if we denote the distance between plane Γ_A and the left side of the defect as z_l then the reflection

coefficient Λ for mode (m, n) [in the frequency domain only] is defined as

$$\Lambda^{(m,n)} = \frac{\left| B^{(m,n)} u_{1q-}^{(m,n)} e^{ik\gamma^{(m,n)}z_l} \right|}{\left| A^{(m_l,n_l)} u_{1q+}^{(m_l,n_l)} e^{-ik\gamma^{(m,n)}z_l} \right|}, \quad q = \theta \text{ or } z. \tag{16}$$

The reflection coefficient Λ is thus defined by normalising a reflected mode (m, n) by an incident mode (m_l, n_l), where the incident mode is determined by the choice of excitation, which will be either torsional (θ) or longitudinal (z). That is, if the incident mode is $T(0, 1)$ then $q = \theta$, and if it is $L(0, 2)$ then $q = z$. Building in the appropriate torsional or longitudinal displacements into Eq. (16) thus permits the comparison with measurements taken with $T(0, 1)$ and $L(0, 2)$ incident modes.

3. Model validation

The three dimensional model is validated here by comparing predictions against those available for two dimensional problems. Accordingly, the SAFE method is validated first, and then predictions obtained using the hybrid method for a coated pipe are compared against those in the literature for an axisymmetric defect. In the validation that follows, as well as the results presented in following sections, six noded triangular isoparametric elements are used for planes Γ_A and Γ_B, and ten noded tetrahedral isoparametric elements are used for Ω_2. The numerical model is programmed in MATLAB and executed on a computer with 12 CPU cores and a total accessible RAM of 128 GB. Parallelisation techniques are used so that the problem is solved in parallel for 12 frequencies at a time. Further, the properties of the coating follow the definition of Barshinger and Rose [3], so that the shear torsional and longitudinal bulk wave velocities are given as $c_{T_c} = 1/[1/\tilde{c}_T - i\tilde{\alpha}_T]$ and $c_{L_c} = 1/[1/\tilde{c}_L - i\tilde{\alpha}_L]$, respectively. Here, $\tilde{c}_T$ and $\tilde{c}_L$ denote the shear and longitudinal phase velocities, and $\tilde{\alpha}_T$ and $\tilde{\alpha}_L$ represent attenuation in the coating.

3.1. SAFE method for a coated pipe

The two dimensional SAFE method presented here is valid for a waveguide of any cross-sectional geometry, although in this article we restrict application to an axisymmetric pipe. A two dimensional solution is used as this makes the application of the hybrid method that follows more straightforward, especially when using flexural modes to enforce the matching conditions over Γ_A and Γ_B. Accordingly, the two dimensional SAFE solution is validated first by comparison against the independent one dimensional predictions for an axisymmetric pipe reported by Marzani et al. [12]. The pipe studied by Marzani et al. was filled with a viscoelastic material, rather than coated on the outside, and the pipe had an inner radius of 6.8 mm and an outer radius of 7.5 mm. The properties of the copper substrate are $c_{T_p} = 2240$ m/s, with a density $\rho_p = 8900$ kg/m^3. For the viscoelastic filling, $\tilde{c}_T = 430$ m/s, $\tilde{\alpha}_T = 0.5 \times 10^{-3}$ s/m and $\rho_C = 970$ kg/m^3. For the purposes of comparison, the two dimensional SAFE predictions are generated using 1288 nodes in the copper substrate and 3261 nodes in the viscoelastic filling, so that $p_{1x} = p_{1y} = p_{1z} = 4357$ and the total degrees of freedom p_1 = 13,071. In Fig. 2 predictions are compared against those found by Marzani et al. [12] for the $T(0, 1)$ mode only, and it is seen that the current method delivers predictions that overlay those of Marzani et al. This provides evidence that the two dimensional SAFE method is working correctly, at least for this problem. Further validation was obtained by comparing predictions against the one dimensional model of Kirby et al. [22,23] and similar levels of agreement for longitudinal modes were also
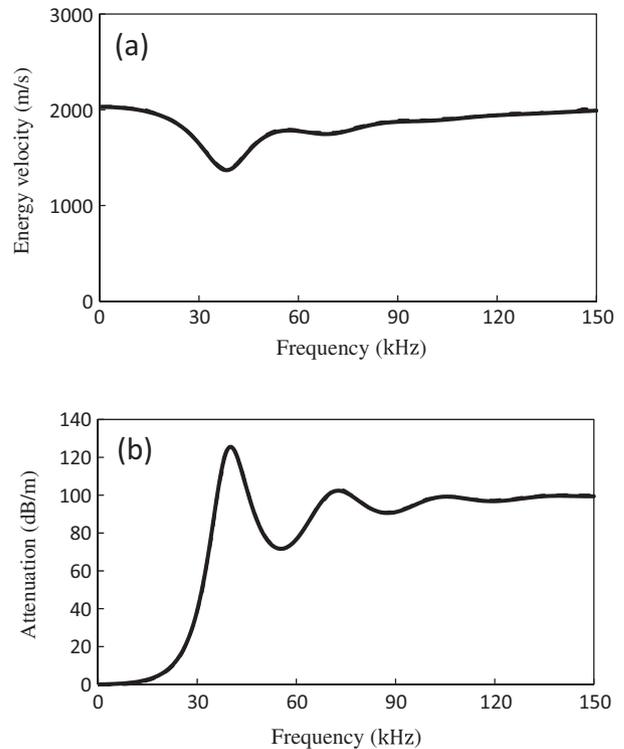
Fig. 2. Comparison between two dimensional SAFE predictions and those of Marzani et al. [12] for $T(0, 1)$: —, current SAFE model, – – –, one dimensional SAFE model of Marzani et al.; (a) energy velocity, (b) attenuation; (solutions overlay one another).

observed (not shown here), provided of course that sufficient nodes were included in the two dimensional model.

3.2. Hybrid method for a coated pipe

There are far fewer results in the literature for pipes containing discontinuities and so validation against existing predictions is much more difficult for the hybrid method. The only suitable studies for coated pipes are the axisymmetric investigations of Kirby et al. [22,23], and so the three dimensional hybrid model is validated here by comparing predictions against a two dimensional model for an axisymmetric defect. Accordingly, the square defect used by Kirby et al. [22,23] is chosen, which is axisymmetric and uniform in the axial direction with a length of 15 mm, so that it cuts through the coating and penetrates 2.8 mm into the steel pipe substrate. The inner radius of the steel pipe is 39 mm and the outer radius of pipe substrate is 44.65 mm, with a coating thickness of 1.5 mm. The properties of the steel substrate are $c_{T_p} = 3260$ m/s, $c_{L_p} = 5960$ m/s, with a density $\rho_p = 8030$ kg/m^3. For the coating, $\tilde{c}_T = 750$ m/s, $\tilde{c}_L = 1860$ m/s, $\tilde{\alpha}_T = 3.9 \times 10^{-3}$ s/m and $\tilde{\alpha}_L = 0.023 \times 10^{-3}$ s/m, and $\rho_C = 1200$ kg/m^3. At each frequency, the two dimensional SAFE predictions for this problem are generated using 6680 nodes in the steel substrate and 3892 nodes in the viscoelastic coating, so that $p_{1x} = p_{1y} = p_{1z} = 9820$ and $p_1 = 29,460$. The hybrid model then uses 200 of those modes found in the SAFE solution, so that $m_1 = 200$ and for the finite element mesh in region Ω_2, $p_2 = 489,228$.

In Fig. 3(a) and (b) the reflection coefficients for an axisymmetric defect are compared for excitation by $T(0, 1)$ and $L(0, 2)$ incident modes, respectively. The reflection coefficient used in these figures is the one defined in the article by Duan and Kirby [21]. It is seen in Fig. 3(a) and (b) that the agreement between the two and three
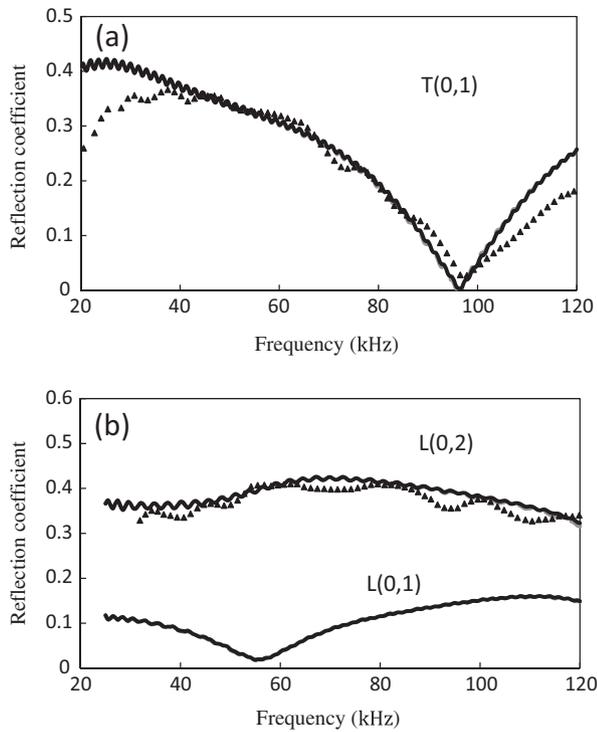
Fig. 3. Reflection coefficients for (a) the $T(0,1)$ mode and (b) the $L(0,2)$ mode incident upon an axisymmetric defect: —, current three dimensional model; – – –, two dimensional axisymmetric models of Kirby et al. [22,23]; ▲, Experiment [22,23].

dimensional approach is very good, and agreement was achieved to an accuracy of at least two decimal places over the frequency range shown. Of course, these two models should agree very well as they are solving the same problem, however the results in Fig. 3 illustrate that it is possible to implement a three dimensional model and deliver accurate predictions over a wide frequency range in a reasonable computational time.

4. Frequency domain: results and discussion

The hybrid method reported in the previous sections is designed to allow a more detailed investigation into wave propagation in a coated pipe with a view to optimising the performance of commercial LRUT devices. The most significant problem encountered in experimental testing is that the coating attenuates the incident and reflected signal and so one finds it difficult to detect defects that are a relatively long distance from the source of excitation. However, it is not known if the coating significantly affects the way in which the waves are scattered by a defect, or how the coating affects the interpretation of the returning pulse in the time domain. Accordingly, the following sections address these questions and attempt to guide LRUT in coated pipes towards a more optimal approach. This is best achieved by first analysing the influence of the coating in the frequency domain, which is then followed in the next section by an investigation in the time domain. The frequency domain analysis that follows splits into two parts, the first examines the behaviour of the coated pipe eigenmodes, whereas the second part examines scattering from a defect. In the example that follows the coated section of the pipe has the following properties (unless otherwise specified): the pipe substrate is made from steel and the coating is the same viscoelastic material as that described in Section 3.2. The inner radius of the pipe is

39 mm, the outer radius of the steel substrate is 44.65 mm, and a reference coating with a thickness of 1.5 mm is chosen.

4.1. Mode shapes for a coated pipe

To gain an insight into the way in which each mode propagates in a coated pipe it is helpful to start by examining the shape of each eigenmode, and in particular the effect the coating has on each mode shape. Accordingly, in Fig. 4(a)–(c) the mode shape for a number of different modes is presented. Note that only a finite number of least attenuated modes are analysed here so that those modes with high levels of attenuation over the frequency range of interest in LRUT (roughly 20–100 kHz) are neglected. Moreover, in Fig. 4 these modes are grouped together according to their mode shape so that three different families of modes are presented. Thus, in Fig. 4(a) the family containing $T(0,1)$, $F(1,2)$, $F(2,2)$ and $F(3,2)$ is presented [hereafter referred to as the $T(0,1)$ family]; Fig. 4(b) contains $L(0,2)$, $F(1,3)$, $F(2,3)$ and $F(3,3)$ [the $L(0,2)$ family]; and Fig. 4 (c) contains $L(0,1)$, $F(1,1)$, $F(2,1)$ and $F(3,1)$ [the $L(0,1)$ family]. Note that at 70 kHz, $T(0,1)$ overlays $F(1,2)$ and $L(0,1)$ overlays $F(1,1)$ in Fig. 4. The mode shapes illustrated in Fig. 4 are important
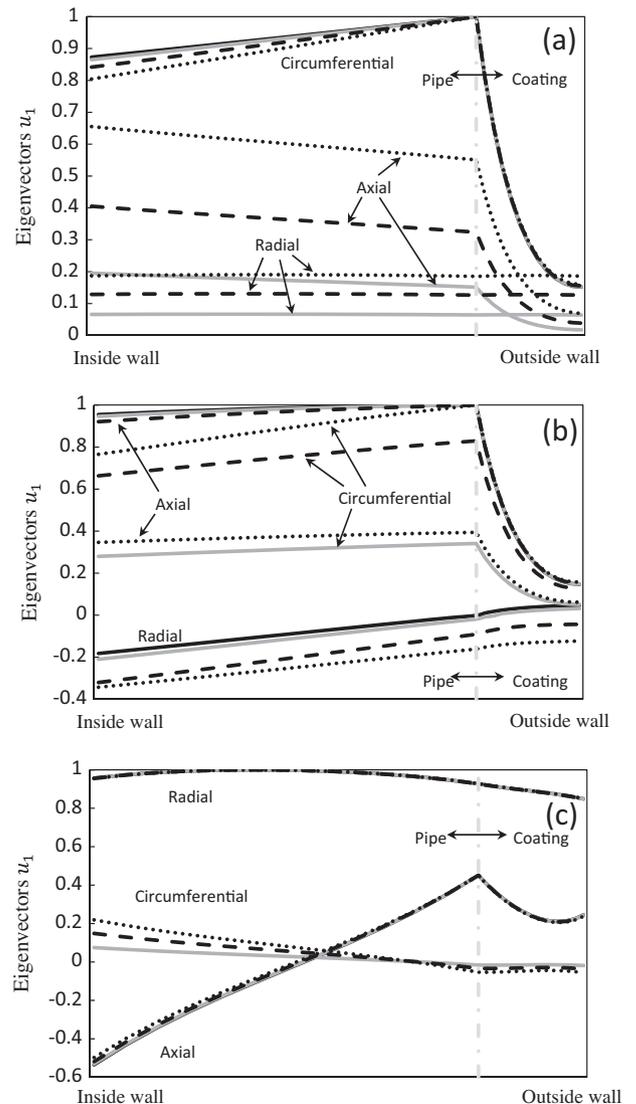
Fig. 4. Mode shapes for 3 in. schedule 40 coated pipe at 70 kHz. (a) —, $T(0,1)$; —, $F(1,2)$; – – –, $F(2,2)$; · · ·, $F(3,2)$. (b) —, $L(0,2)$; —, $F(1,3)$; – – –, $F(2,3)$; · · ·, $F(3,3)$. (c) —, $L(0,1)$; —, $F(1,1)$; – – –, $F(2,1)$; · · ·, $F(3,1)$.

in understanding how each mode behaves when a coating is added. This is most apparent with the large displacement drop seen within the coating for the circumferential eigenvector in Fig. 4(a). This has important ramifications for the use of torsional modes in LRUT because these modes require excitation in the circumferential direction. Furthermore, if one attaches a commercial LRUT device directly onto the outside of the coating and attempts to drive the $T(0,1)$ family, then the device is likely to find it difficult to transfer significant levels of energy into this family of modes and so there will be only a limited range over which the technique will work. Thus, if one insists on using the $T(0,1)$ family to find defects in coated pipes one must at least remove the coating before attaching the test equipment.

In Fig. 4(b) it is seen that for the $L(0,2)$ family the displacement drop in the coating region is smaller than that seen for the $T(0,1)$ family. It is significant that this is observed also for $L(0,2)$, which is normally the excitation mode of choice if one is using longitudinal modes, and this drop is not as severe as that seen for $T(0,1)$. Therefore, these figures illustrate that $L(0,2)$ is likely to be a better choice for LRUT when compared to $T(0,1)$, although the displacement drop for the $L(0,2)$ family is still significant and it appears prudent also to remove the coating when attempting to test sections of coated pipe. It is interesting to note that in Fig. 4(c) the $L(0,1)$ family is actually the best choice for the study of coated pipes. However, there are known to be practical difficulties when attempting to excite $L(0,1)$, as it is harder to focus the energy into this mode when compared to $L(0,2)$. Moreover, in the frequency range of interest $L(0,1)$ is also more dispersive than $L(0,2)$ (see also Fig. 6(a) in Section 4.3) and so it is not normally favoured. Nevertheless, the results presented in Fig. 4 indicate that if these practical problems could be overcome, the $L(0,1)$ family is the most attractive alternative for studying scattering from defects in coated pipes.

4.2. Attenuation in a coated pipe

The influence of the coating on mode shape seen in Fig. 4 may also be observed in the relative attenuation of each mode, and this is shown in Fig. 5(a)–(d) for coating thicknesses of 1.5 mm, 3 mm and 5 mm. It can be seen in Fig. 5 that the attenuation of modes that sit within each family is similar to one another, especially as one moves away from the equivalent modal cut-on frequency for an uncoated pipe. This similarity in attenuation is caused by the similarity in mode shape seen in Fig. 4. It is interesting also to observe the effect of changing the coating thickness and here the $T(0,1)$ family is seen to be especially sensitive to coating thickness at lower frequencies. This behaviour indicates that the $T(0,1)$ family is potentially more sensitive to changes in material properties in the low frequency region, and this coincides with the frequency range where one may wish to attempt measurements on coated pipes (on the basis that one would expect lower levels of attenuation at lower frequencies). Moreover, the sensitivity of $T(0,1)$ is seen to be greater than that for $L(0,2)$, which exhibits consistently lower levels of attenuation, especially at low frequencies. This
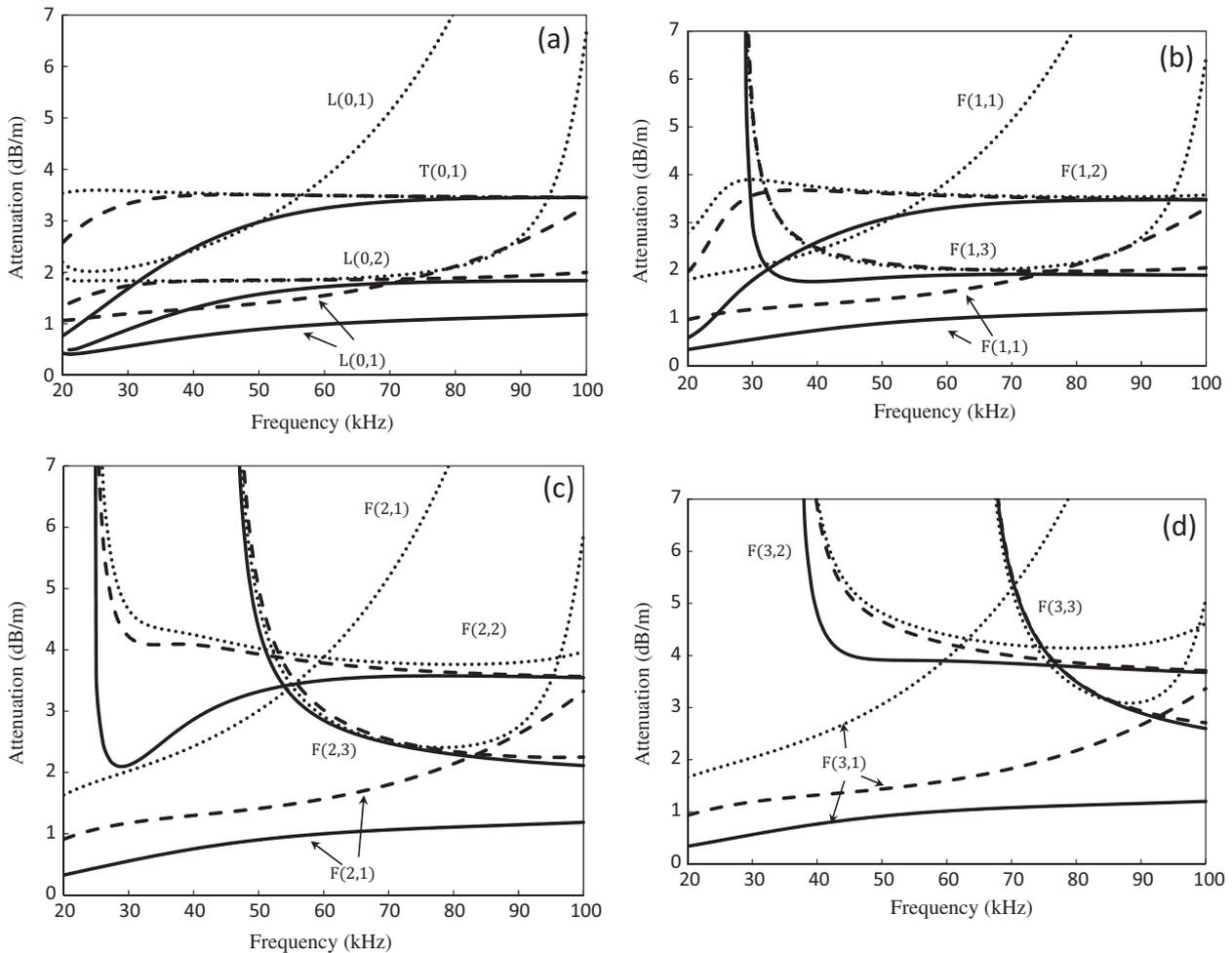
Fig. 5. Attenuation in pipe coated with viscoelastic bitumen. —, 1.5 mm coating thickness; – – –, 3 mm coating thickness; ···, 5 mm coating thickness.

provides further evidence to support the use of longitudinal modes in LRUT on coated pipes.

4.3. Energy velocity in coated pipes

The relative attenuation of each mode is clearly very important when choosing the optimum strategy for LRUT in coated pipes. Another important quantity is the energy velocity of the wave as it travels along the pipe. The energy velocity is used extensively in uncoated pipes, where it is known as the group velocity. Energy velocity is used in the time domain to aid in separating different modes, as it enables one to calculate the time of flight of the propagating mode of interest. The energy velocity is defined in Eq. (8), and in Fig. 6 the energy velocity with and without a coating is compared for the three modal families. To further investigate the effects of a coating, the energy velocity is also plotted for three different coating thicknesses, and here it is evident that the energy velocity of each mode remains largely unaffected by the presence of the coating, at least over the frequency range covered here. This demonstrates that the action of the coating is largely restricted to damping the energy carried by the wave and that it does not add significant levels of mass or stiffness to the system. Furthermore, one may see that $T(0,1)$ and $L(0,2)$ retain their non-dispersive characteristics over the frequency range of interest here, and so one may conclude that for LRUT the time of flight techniques used to separate modes in uncoated pipes are applicable also to coated pipes. Of course, the time domain response seen for a coated pipe will be different because of modal attenuation, and this is investigated in the next section.

4.4. Scattering from a non-axisymmetric defect

The analysis undertaken so far investigates the influence of the coating on the properties of individual modes. This includes the mode shape and wavenumber, so that if one returns to Eqs. (13) and (14) this relates to the eigenvector u_1, and the eigenvalue γ. However, this article is also interested in the effect of the coating on the way in which a wave scatters from a defect. In terms of Eqs. (13) and (14) this translates into the effect of the coating on the modal amplitudes A, B and C. To do this, the scattering from a non-axisymmetric defect is investigated, as this is more representative of actual defects found in the field when compared, say, to the axisymmetric defects studied by Kirby et al. [22,23]. To investigate the influence of the coating on the way in which a defect scatters the incident wave, scattering from a non-axisymmetric defect is studied here by comparing reflection coefficients obtained with and without a coating at a location immediately adjacent to the start of the defect. This choice of location is convenient because it avoids the additional attenuation imparted by the coating as one moves away from the defect, and so isolates the effect of the coating on the modal amplitudes. For this problem the properties of the coating and the substrate are the same as those described at the start of this section; the non-axisymmetric defect then extends 10% around the circumferential direction of the pipe, penetrates
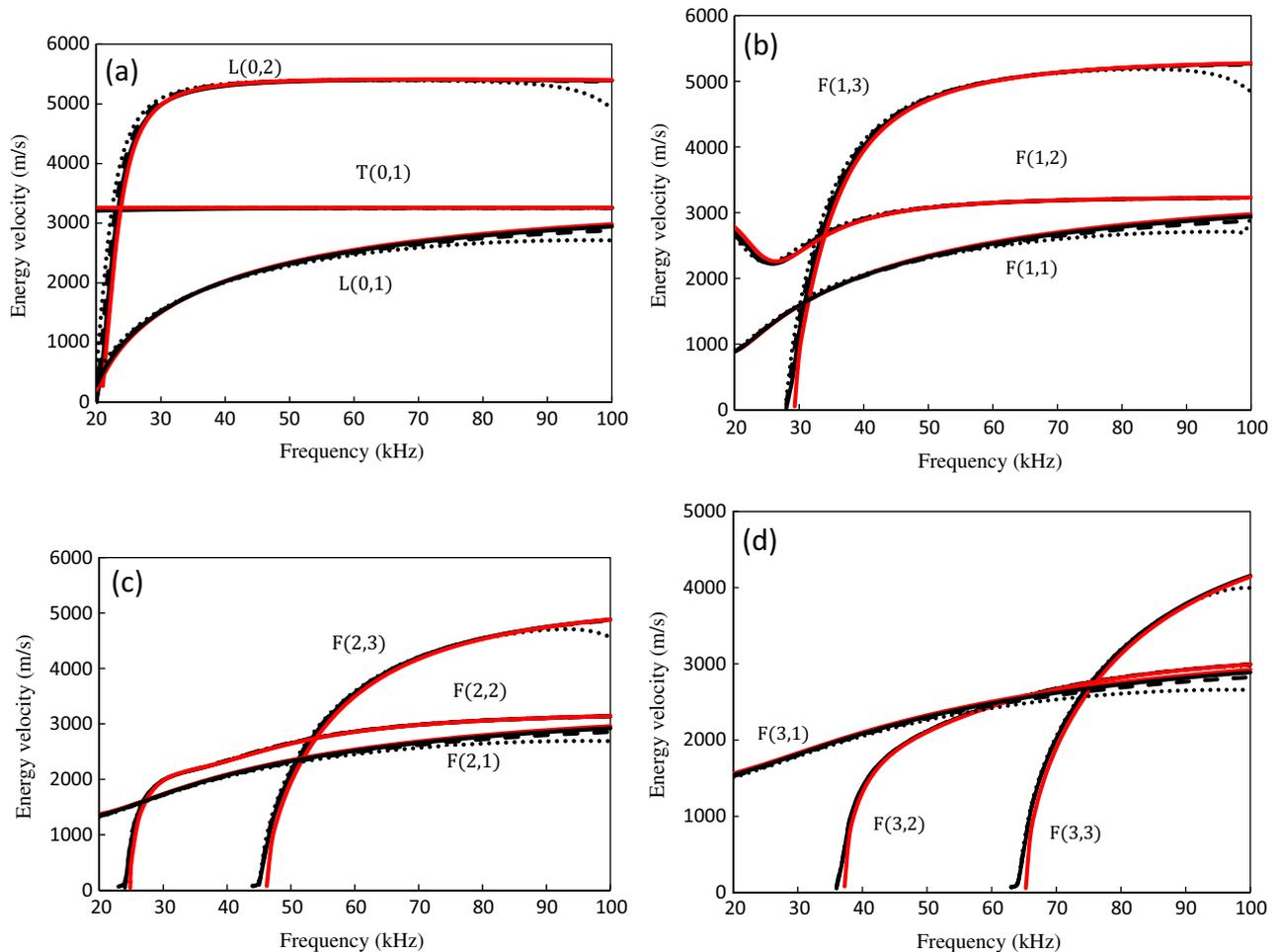
Fig. 6. Comparison between energy velocities for an uncoated and coated pipe. —, uncoated pipe; —, 1.5 mm coating thickness; – – –, 3 mm coating thickness; ⋯, 5 mm coating thickness.

the coating and goes 50% into the pipe wall (2.8 mm), and has a length of 2.5 mm. The area ratio of the defect (cross-sectional area of the defect compared to cross-sectional area of the pipe without coating) is approximately 5%.

Fig. 7(a) and (b) shows the reflection coefficients for the $T(0,1)$ and $L(0,2)$ family of modes with excitation from $T(0,1)$ and $L(0,2)$ modes, respectively. The reflection coefficients of flexural modes are calculated using the maximum displacement values around the circumference of the pipe. In Fig. 8(a) and (b) a similar comparison is also made but this time for a different defect, which has the same length and depth as the defect in Fig. 7, but in Fig. 8 the defect extends around 50% of the pipe circumference. The area ratio of the defect shown in Fig. 8 is therefore 25%. It is clear in both figures that the reflection coefficients with and without a coating are very similar, and this means that the modal amplitudes are very similar as well. Thus, the coating does not affect the way in which the wave is scattered by the defect, apart from the additional change in geometry caused by the thickness of the coating itself. That is, there is no additional mode conversion taking place because of the presence of the coating, and the influence of the coating is restricted to the attenuation of energy as the wave propagates down the pipe. This is an important result as it means that when undertaking experimental measurements one need only account for the effect of the coating on modal attenuation, without the need to consider additional complexities such a change in mode conversion and/or energy velocity. Thus, one does not need to model a three dimensional coated pipe if the coating is relatively thin, instead it is necessary only to model an uncoated pipe and simply to factor in modal attenuation after undertaking a SAFE solution for a coated pipe.

It is also observed in Figs. 7 and 8 that the reflection coefficient for flexural modes is stronger than for the equivalent $T(0,1)$ or $L(0,2)$ mode. However, it should be remembered that flexural modes are normally more dispersive than axisymmetric modes (see Figs. 5 and 6) and so in the time domain their modal amplitude will be reduced by dispersion as they propagate along the pipe, which means that the reflection coefficient for flexural modes is likely to be significantly reduced at locations well away from the defect. Note also that the sharp spikes seen in Figs. 7 and 8 are caused by modal cut-on in the uncoated pipe; the additional damping provided by the coating is seen to reduce the amplitude of these peaks and in experiments one may expect to see this amplitude reduced still further by additional damping in the steel substrate that is not accounted for in this model. Figs. 7 and 8 also illustrate how a change in shape of this type of defect significantly alters the energy distribution among flexural modes.

5. Time domain: results and discussion

The previous section investigated wave propagation in the frequency domain; however, LRUT is normally undertaken in the time domain because this is a convenient way to analyse scattering from a defect. Operating in the time domain does, however, mean that the user is faced with the task of interpreting a complex signal and understanding these signals is often a significant challenge. To investigate the interpretation of these signals it is important to generate predictions in the time domain, and here we will follow the method of Duan and Kirby [21]. Moreover, time domain predictions have yet to appear for coated pipes and so in view of the practical importance of time domain signatures this article also shows how time domain predictions may be generated and reviews the way in which the coating is likely to influence the interpretation of time domain data.

Time domain predictions are generated here using an incident pulse consisting of a 10 cycle Hanning windowed sinusoidal wave with a centre frequency of 70 kHz. This pulse is then transformed into the frequency domain using a discretised Fourier transform with 1836 discrete frequencies extending from 35 kHz to
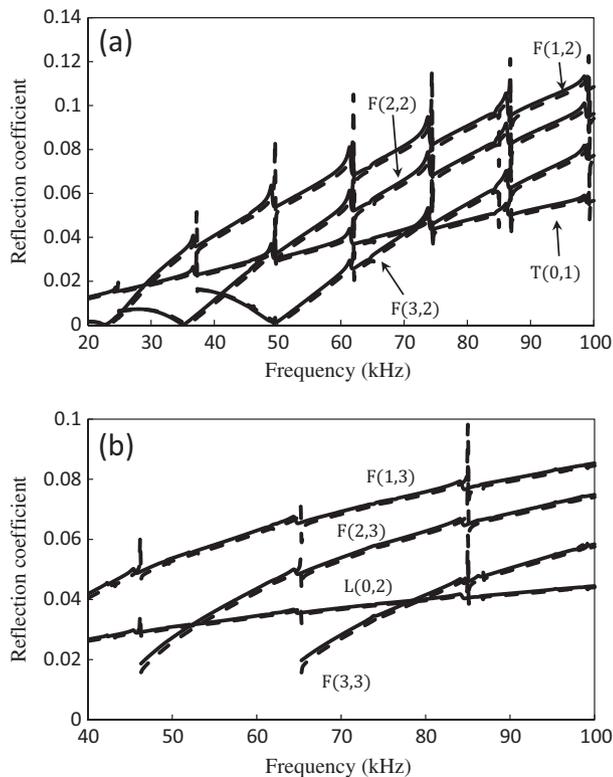
Fig. 7. Reflection coefficients for (a) the $T(0,1)$ mode and (b) the $L(0,2)$ mode incident upon a 5% area ratio non-axisymmetric defect: —, coated pipe; – – –, uncoated pipe.
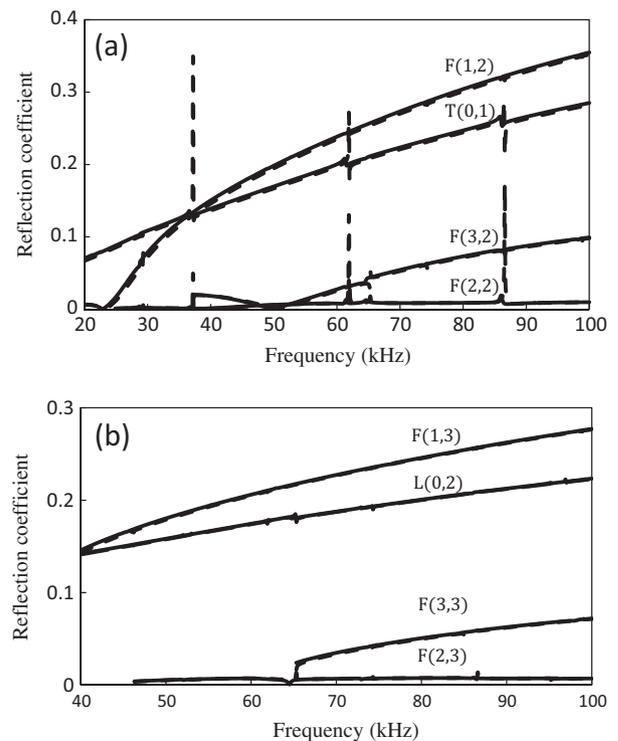
Fig. 8. Reflection coefficients for (a) the $T(0,1)$ mode and (b) the $L(0,2)$ mode incident upon a 25% area ratio non-axisymmetric defect: —, coated pipe; – – –, uncoated pipe.
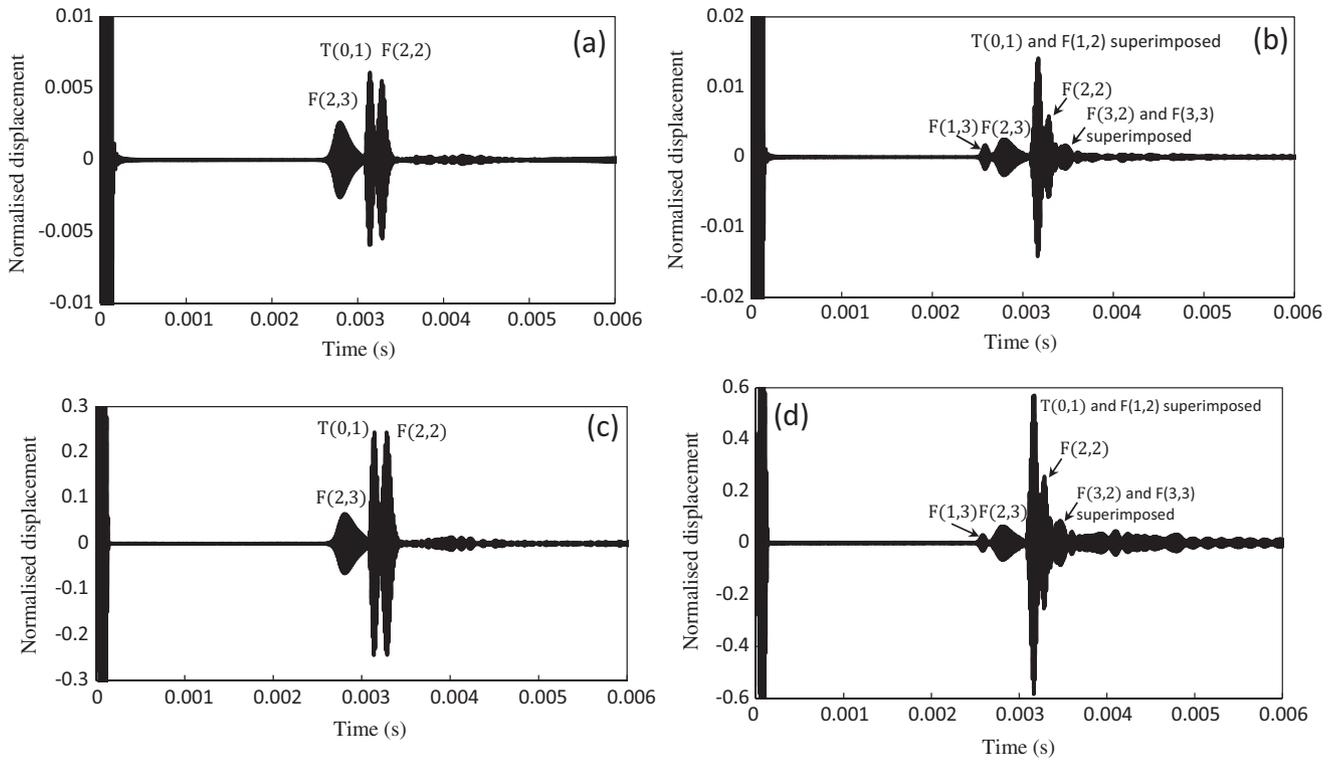
Fig. 9. Predicted circumferential displacement for the $T(0,1)$ mode incident upon a non-axisymmetric defect. (a) $x = R$; (b) $y = R$, coated; (c) $x = R$; (d) $y = R$, uncoated.

105 kHz in increments of 38.15 Hz. The complex amplitude obtained for the pulse at each frequency is then used as the incident modal amplitude in Eq. (15). Following the solution of Eq. (15) at each discrete frequency, an inverse Fourier transform is used to generate the time domain predictions. The number of discrete frequencies chosen, as well as the size of these frequency increments, are designed to minimise numerical noise whilst at the same time maintaining an acceptable solution time.

The sample problem investigated in this section is based on the non-axisymmetric scattering problem studied in the previous section. Thus, the defect extends around 20% of the circumference and penetrates through the steel substrate and has a length of 2.5 mm. All other parameters for the pipe and the coating remain the same as those detailed at the start of Section 3.2. Analysing scattering from a defect in the time domain is complicated by modes travelling at similar energy velocities so that they overlap one another. Therefore, in order to separate out modes in the figures that follow, the scattered signal is calculated at a distance of 5 m from the defect and at two separate circumferential locations, $x = R, y = 0$ and $x = 0, y = R$, where R is the outer radius of the uncoated pipe. Note that $y = R$ is directly opposite to the defect, see Fig. 1. These two circumferential locations are also referred to as 'x direction' and 'y direction' in Figs. 6 and 7 of Ref. [21]. Accordingly, in Fig. 9 the predicted displacement at $x = R$ and $y = R$ is shown for scattering by the non-axisymmetric defect in a coated and uncoated pipe at a distance of 5 m from the defect. The defect is excited using $T(0,1)$ and so only the circumferential displacement is shown in Fig. 9. In this figure, the amplitude of the reflected pulse is seen to significantly reduce following the addition of the coating, which is what one would expect to see following the analysis in the previous section. Of course, the size of this reduction is largely dictated by the effective distance between source and receiver, which in this case is 10 m. However, it is noted that the results in the previous section indicate that no additional mode

conversion takes place because of the presence of the coating and so one may infer that the drop in amplitude seen in Fig. 9 is solely caused by modal attenuation. For example, in this problem the attenuation of $T(0,1)$ at 70 kHz is 3.44 dB/m, which gives a sound power reduction of 34.4 dB over 10 m. If one reads the attenuation directly from Fig. 9 then the value obtained for $T(0,1)$ is 32.3 dB. Thus the two figures are close enough to one another to support previous observations regarding the influence of the coating on mode conversion, with the small difference seen here likely to be caused by truncation and discretisation errors in the discrete Fourier transform.

It is well known that problems are found when attempting to detect defects in coated pipes, and these problems are clearly evident in Fig. 9. Whilst the dispersive behaviour of each mode changes very little after adding the coating, at least within this frequency range, the amplitude of each mode reduces significantly and this is why the use of $T(0,1)$ on coated pipes is likely to be very difficult. However, it was shown in the previous section that $L(0,2)$ may be more useful and so in Fig. 10 the equivalent response of a pipe excited by $L(0,2)$ is shown. Again, the amplitude of each mode is seen to reduce following the addition of the coating, although it is noticeable that this also means that the noisy "tail" is also damped down. Clearly, the reflected amplitude of the $L(0,2)$ family is higher than that seen for $T(0,1)$, and here the attenuation of $L(0,2)$ is now 17.2 dB when compared to 32.3 dB for $T(0,1)$. This difference in amplitude is significant in the context of real experimental measurements, although the figures seen here are of course relevant only to this type of problem. Obviously, if one changes the type of defect, the coating and/or the distance between the defect and the receiver then these figures will change, however the results obtained in the previous section illustrate that the properties of the $L(0,2)$ mode should normally deliver lower levels of attenuation, at least over the frequency range typically associated with LRUT.
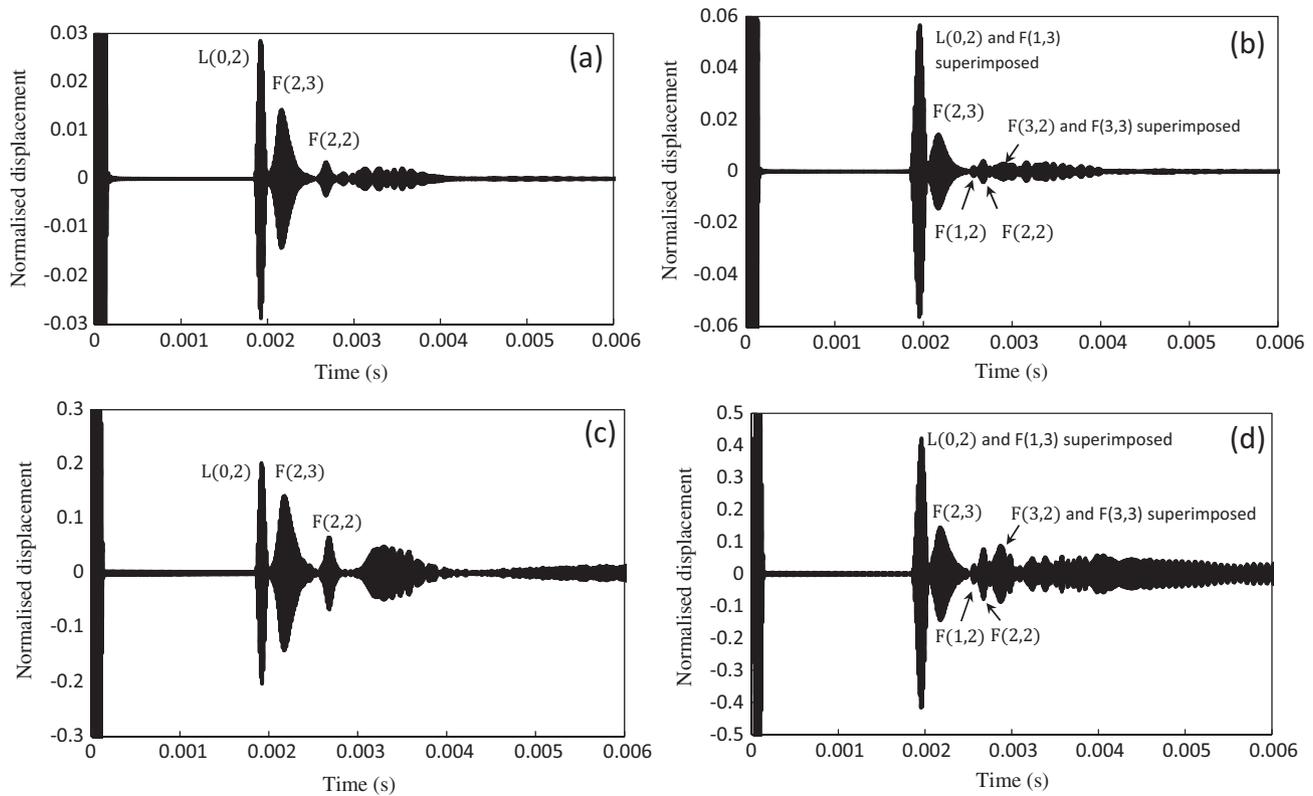
Fig. 10. Predicted axial displacement for the $L(0,2)$ mode incident upon a non-axisymmetric defect. (a) $x = R$; (b) $y = R$, coated; (c) $x = R$; (d) $y = R$, uncoated.

The time domain signatures shown in Figs. 9 and 10 illustrate that, in principle, there should be little difference in the complexity of a pulse reflected from a defect in a coated or uncoated pipe. However, this is not normally the experience in real experiments taken on pipes that have been *in situ* for a number of years. It is likely, therefore, that additional levels of complexity are caused by an increase in noise that arises from the coating itself. For example, it is possible that over time most coatings in real applications will start to degrade, so that small inhomogeneities appear, as well as delamination and/or de-bonding from the pipe. These imperfections will impart additional levels of attenuation, as well as introduce additional scattering. Thus, it is these imperfections that are likely to be the cause of additional problems with LRUT in coated pipes and not issues such as mode conversion or additional dispersion. Accordingly, it remains to be seen how the suggested improvements identified in this article are affected by imperfections within the coating of real pipe systems.

6. Conclusions

This article has used a hybrid SAFE-finite element based method to analyse the scattering of guided waves from non-axisymmetric defects in coated pipes. It is shown that predictions in the time and frequency domain can be generated for an infinite pipe using relatively modest computational facilities. The predictions obtained from this model indicate that the torsional $[T(0,1)]$ family of modes have high levels of attenuation for the frequency range normally used in LRUT (20–120 kHz); moreover, the levels of attenuation for torsional modes are very sensitive to the thickness of the coating in the low frequency region. The longitudinal family of modes $[L(0,2)]$ are seen to have lower levels of attenuation and so it is observed that for the viscoelastic coating studied here the longitudinal family of modes will have a longer range when compared to torsional modes. It is also observed that the energy

velocity for each mode is very similar to the group velocity of the equivalent mode for an uncoated pipe. This means that the coating does not introduce additional levels of dispersion beyond what is normally observed for uncoated pipes, at least over the typical frequency range used in LRUT. This is an important result when attempting to interpret signals obtained in the time domain.

The frequency and time domain predictions generated for a non-axisymmetric defect demonstrate that scattering from the defect remains largely unaffected by the presence of the coating. In other words, there is no additional mode conversion occurring in the pipe because of the presence of the coating, and the only effect a coating has on scattering is caused by the small change in the geometry of the defect, which may be neglected for most coatings. Thus, it appears reasonable to conclude that the only significant effect that needs to be considered is the attenuation the coating imparts on each mode. Therefore, if one wishes to model the effect of a viscoelastic material on scattering from a defect in a pipe or other structure then provided the thickness of the material is small compared to the thickness of the substrate, it is sufficient to model only the uncoated structure and to account for the influence of the viscoelastic material through modal attenuation, which may readily be found using the SAFE method. Furthermore, when undertaking experimental measurements the methods currently used in LRUT may also be retained, such as the interpretation of the returning signal using group velocity data, and it is necessary only to correct for the attenuation of each mode when reviewing echoes from a defect in the time domain.

The theoretical method developed here is designed to take advantage of the long slender structures found in pipelines. This has enabled numerical predictions to be generated efficiently in the frequency and the time domain using relatively modest computer facilities. However, in the future it may be interesting to investigate whether the computational efficiency of this method

may be increased through the introduction of higher order elements such as those described by Ostachowicz el al. [17] and/or through additional optimisation of the finite element mesh.

Appendix A

$$
\mathbf{P}_{p,c} = \begin{bmatrix} \mathbf{0} & \mathbf{0} & \mathbf{0} & \mathbf{Z}_{41p,c}^T & \mathbf{Z}_{51p,c}^T & \mathbf{0} \\ \mathbf{0} & \mathbf{0} & \mathbf{0} & \mathbf{Z}_{51p,c} & \mathbf{Z}_{52p,c} & \mathbf{0} \\ \mathbf{0} & \mathbf{0} & \mathbf{0} & \mathbf{0} & \mathbf{0} & \mathbf{Z}_{63p,c}^T \\ \mathbf{Z}_{41p,c} & \mathbf{Z}_{51p,c}^T & \mathbf{0} & \mathbf{0} & \mathbf{0} & \mathbf{Z}_{64p,c}^T \\ \mathbf{Z}_{51p,c} & \mathbf{Z}_{52p,c} & \mathbf{0} & \mathbf{0} & \mathbf{0} & \mathbf{Z}_{65p,c}^T \\ \mathbf{0} & \mathbf{0} & \mathbf{Z}_{63p,c} & \mathbf{Z}_{64p,c} & \mathbf{Z}_{65p,c} & \mathbf{0} \end{bmatrix} \tag{A1}
$$

$$
\mathbf{S}_{p,c} = \begin{bmatrix} \mathbf{Z}_{41p,c}^T & \mathbf{Z}_{51p,c}^T & 0 & 0 & 0 & 0 \\ \mathbf{Z}_{51p,c} & \mathbf{Z}_{52p,c}^T & 0 & 0 & 0 & 0 \\ 0 & 0 & \mathbf{Z}_{63p,c}^T & 0 & 0 & 0 \\ 0 & 0 & 0 & \mathbf{Z}_{44p,c} & 0 & 0 \\ 0 & 0 & 0 & 0 & \mathbf{Z}_{44p,c} & 0 \\ 0 & 0 & 0 & 0 & 0 & \mathbf{Z}_{66p,c} \end{bmatrix} \tag{A2}
$$

$$
\mathbf{Z}_{41p,c} = \rho_{p,c}\left[\left(c_{Lp,c}^2 - c_{Tp,c}^2\right)\mathbf{K}_{xp,c} + c_{Tp,c}^2\mathbf{K}_{1p,c} - \omega^2\mathbf{K}_{2p,c}\right] \tag{A3}
$$

$$
\mathbf{Z}_{51p,c} = \rho_{p,c}\left[\left(c_{Lp,c}^2 - 2c_{Tp,c}^2\right)\mathbf{K}_{xyp,c}^T + c_{Tp,c}^2\mathbf{K}_{xyp,c}\right] \tag{A4}
$$

$$
\mathbf{Z}_{52p,c} = \rho_{p,c}\left[\left(c_{Lp,c}^2 - c_{Tp,c}^2\right)\mathbf{K}_{yp,c} + c_{Tp,c}^2\mathbf{K}_{1p,c} - \omega^2\mathbf{K}_{2p,c}\right] \tag{A5}
$$

$$
\mathbf{Z}_{63p,c} = -\rho_{p,c}\left(c_{Tp,c}^2\mathbf{K}_{1p,c} - \omega^2\mathbf{K}_{2p,c}\right) \tag{A6}
$$

$$
\mathbf{Z}_{64p,c} = \rho_{p,c}ik\left[-\left(c_{Lp,c}^2 - 2c_{Tp,c}^2\right)\mathbf{K}_{3p,c} + c_{Tp,c}^2\mathbf{K}_{3p,c}^T\right] \tag{A7}
$$

$$
\mathbf{Z}_{65p,c} = \rho_{p,c}ik\left[-\left(c_{Lp,c}^2 - 2c_{Tp,c}^2\right)\mathbf{K}_{4p,c} + c_{Tp,c}^2\mathbf{K}_{4p,c}^T\right] \tag{A8}
$$

$$
\mathbf{Z}_{44p,c} = -\rho_{p,c}c_{Tp,c}^2k^2\mathbf{K}_{2p,c} \tag{A9}
$$

$$
\mathbf{Z}_{66p,c} = \rho_{p,c}c_{Lp,c}^2k^2\mathbf{K}_{2p,c} \tag{A10}
$$

$$
\mathbf{K}_{1p,c} = \int_{\Gamma_{1p,c}} \nabla\mathbf{N}^T\nabla\mathbf{N}d\Gamma_{1p,c} \quad \text{and} \quad \mathbf{K}_{2p,c} = \int_{\Gamma_{1p,c}} \mathbf{N}^T\mathbf{N}d\Gamma_{1p,c} \tag{A11a, b}
$$

$$
\mathbf{K}_{3p,c} = \int_{\Gamma_{1p,c}} \mathbf{N}^T\frac{\partial\mathbf{N}}{\partial x}d\Gamma_{1p,c} \quad \text{and} \quad \mathbf{K}_{4p,c}
$$
$$
= \int_{\Gamma_{1p,c}} \mathbf{N}^T\frac{\partial\mathbf{N}}{\partial y}d\Gamma_{1p,c} \tag{A12a, b}
$$

$$
\mathbf{K}_{xp,c} = \int_{\Gamma_{1p,c}} \frac{\partial\mathbf{N}^T}{\partial x}\frac{\partial\mathbf{N}}{\partial x}d\Gamma_{1p,c} \quad \text{and} \quad \mathbf{K}_{yp,c} = \int_{\Gamma_{1p,c}} \frac{\partial\mathbf{N}^T}{\partial y}\frac{\partial\mathbf{N}}{\partial y}d\Gamma_{1p,c} \tag{A13a, b}
$$

$$
\mathbf{K}_{xyp,c} = \int_{\Gamma_{1p,c}} \frac{\partial\mathbf{N}^T}{\partial x}\frac{\partial\mathbf{N}}{\partial y}d\Gamma_{1p,c} \tag{A14}
$$

Appendix B

$$
\mathbf{G}_{11\pm} = \mathbf{M}_{1x\pm} + \mathbf{M}_{1zxx\pm} + \mathbf{M}_{1y\pm} + \mathbf{M}_{1zyy\pm} + \mathbf{M}_{1z\pm} + \mathbf{M}_{1xxz\pm}
$$
$$
+ \mathbf{M}_{1yyz\pm} \tag{A15}
$$

$$
\mathbf{G}_{21} = \mathbf{Q}_{1x-} + \mathbf{Q}_{1zx-} \tag{A16}
$$

$$
\mathbf{G}_{31} = \mathbf{Q}_{1y-} + \mathbf{Q}_{1zy-} \tag{A17}
$$

$$
\mathbf{G}_{41\pm} = \mathbf{Q}_{1xx\pm} + \mathbf{Q}_{1yy\pm} \mp \mathbf{Q}_{1z\pm} \tag{A18}
$$

$$
\mathbf{G}_{22} = \mathbf{R}_x + \mathbf{R}_1 - \mathbf{R}_2 \tag{A19}
$$

$$
\mathbf{G}_{32} = \mathbf{R}_{xy1}^T + \mathbf{R}_{xy2} \tag{A20}
$$

$$
\mathbf{G}_{42} = \mathbf{R}_{xz1}^T + \mathbf{R}_{xz2} \tag{A21}
$$

$$
\mathbf{G}_{33} = \mathbf{R}_y + \mathbf{R}_1 - \mathbf{R}_2 \tag{A22}
$$

$$
\mathbf{G}_{43} = \mathbf{R}_{yz1}^T + \mathbf{R}_{yz2} \tag{A23}
$$

$$
\mathbf{G}_{44} = \mathbf{R}_z + \mathbf{R}_1 - \mathbf{R}_2 \tag{A24}
$$

$$
\mathbf{G}_{25} = \mathbf{Q}_{3x+} - \mathbf{Q}_{3zx+} \tag{A25}
$$

$$
\mathbf{G}_{35} = \mathbf{Q}_{3y+} - \mathbf{Q}_{3zy+} \tag{A26}
$$

$$
\mathbf{G}_{45} = -\mathbf{Q}_{3xx+} - \mathbf{Q}_{3yy+} + \mathbf{Q}_{3z\tau+} \tag{A27}
$$

$$
\mathbf{G}_{55} = -\mathbf{M}_{3x+} + \mathbf{M}_{3zxx+} - \mathbf{M}_{3y+} + \mathbf{M}_{3zyy+} - \mathbf{M}_{3z+} + \mathbf{M}_{3xxz+}
$$
$$
+ \mathbf{M}_{3yyz+} \tag{A28}
$$

$$
\mathbf{R}_x = \rho_p\left(c_{Lp}^2 - c_{Tp}^2\right)\int_{\Omega_{2p}} \frac{\partial\mathbf{W}^T}{\partial x}\frac{\partial\mathbf{W}}{\partial x}d\Omega_{2p}
$$
$$
+ \rho_c(c_{Lc}^2 - c_{Tc}^2)\int_{\Omega_{2c}} \frac{\partial\mathbf{W}^T}{\partial x}\frac{\partial\mathbf{W}}{\partial x}d\Omega_{2c} \tag{A29}
$$

$$
\mathbf{R}_y = \rho_p\left(c_{Lp}^2 - c_{Tp}^2\right)\int_{\Omega_{2p}} \frac{\partial\mathbf{W}^T}{\partial y}\frac{\partial\mathbf{W}}{\partial y}d\Omega_{2p}
$$
$$
+ \rho_c(c_{Lc}^2 - c_{Tc}^2)\int_{\Omega_{2c}} \frac{\partial\mathbf{W}^T}{\partial y}\frac{\partial\mathbf{W}}{\partial y}d\Omega_{2c} \tag{A30}
$$

$$
\mathbf{R}_{xy1} = \rho_p\left(c_{Lp}^2 - 2c_{Tp}^2\right)\int_{\Omega_{2p}} \frac{\partial\mathbf{W}^T}{\partial x}\frac{\partial\mathbf{W}}{\partial y}d\Omega_{2p}
$$
$$
+ \rho_c(c_{Lc}^2 - 2c_{Tc}^2)\int_{\Omega_{2c}} \frac{\partial\mathbf{W}^T}{\partial x}\frac{\partial\mathbf{W}}{\partial y}d\Omega_{2c} \tag{A31}
$$

$$
\mathbf{R}_{xy2} = \rho_pc_{Tp}^2\int_{\Omega_{2p}} \frac{\partial\mathbf{W}^T}{\partial x}\frac{\partial\mathbf{W}}{\partial y}d\Omega_{2p} + \rho_cc_{Tc}^2\int_{\Omega_{2c}} \frac{\partial\mathbf{W}^T}{\partial x}\frac{\partial\mathbf{W}}{\partial y}d\Omega_{2c} \tag{A32}
$$

$$
\mathbf{R}_{xz1} = \rho_p\left(c_{Lp}^2 - 2c_{Tp}^2\right)\int_{\Omega_{2p}} \frac{\partial\mathbf{W}^T}{\partial x}\frac{\partial\mathbf{W}}{\partial z}d\Omega_{2p}
$$
$$
+ \rho_c(c_{Lc}^2 - 2c_{Tc}^2)\int_{\Omega_{2c}} \frac{\partial\mathbf{W}^T}{\partial x}\frac{\partial\mathbf{W}}{\partial z}d\Omega_{2c} \tag{A33}
$$

$$
\mathbf{R}_{xz2} = \rho_pc_{Tp}^2\int_{\Omega_{2p}} \frac{\partial\mathbf{W}^T}{\partial x}\frac{\partial\mathbf{W}}{\partial z}d\Omega_{2p} + \rho_cc_{Tc}^2\int_{\Omega_{2c}} \frac{\partial\mathbf{W}^T}{\partial x}\frac{\partial\mathbf{W}}{\partial z}d\Omega_{2c} \tag{A34}
$$

$$\mathbf{R}_{yz1} = \rho_{\mathrm{p}}\left(c_{\mathrm{Lp}}^2 - 2c_{\mathrm{Tp}}^2\right)\int_{\Omega_{2\mathrm{p}}}\frac{\partial\mathbf{W^T}}{\partial y}\frac{\partial\mathbf{W}}{\partial z}d\Omega_{2\mathrm{p}}$$
$$+ \rho_{\mathrm{c}}(c_{\mathrm{Lc}}^2 - 2c_{\mathrm{Tc}}^2)\int_{\Omega_{2\mathrm{c}}}\frac{\partial\mathbf{W^T}}{\partial y}\frac{\partial\mathbf{W}}{\partial z}d\Omega_{2\mathrm{c}} \tag{A35}$$

$$\mathbf{R}_{yz2} = \rho_{\mathrm{p}}c_{\mathrm{Tp}}^2\int_{\Omega_{2\mathrm{p}}}\frac{\partial\mathbf{W^T}}{\partial y}\frac{\partial\mathbf{W}}{\partial z}d\Omega_{2\mathrm{p}} + \rho_{\mathrm{c}}c_{\mathrm{Tc}}^2\int_{\Omega_{2\mathrm{c}}}\frac{\partial\mathbf{W^T}}{\partial y}\frac{\partial\mathbf{W}}{\partial z}d\Omega_{2\mathrm{c}} \tag{A36}$$

$$\mathbf{R}_z = \rho_{\mathrm{p}}\left(c_{\mathrm{Lp}}^2 - c_{\mathrm{Tp}}^2\right)\int_{\Omega_{2\mathrm{p}}}\frac{\partial\mathbf{W^T}}{\partial z}\frac{\partial\mathbf{W}}{\partial z}d\Omega_{2\mathrm{p}}$$
$$+ \rho_{\mathrm{c}}(c_{\mathrm{Lc}}^2 - c_{\mathrm{Tc}}^2)\int_{\Omega_{2\mathrm{c}}}\frac{\partial\mathbf{W^T}}{\partial z}\frac{\partial\mathbf{W}}{\partial z}d\Omega_{2\mathrm{c}} \tag{A37}$$

$$\mathbf{R}_1 = \rho_{\mathrm{p}}c_{\mathrm{Tp}}^2\int_{\Omega_{2\mathrm{p}}}\nabla\mathbf{W^T}\nabla\mathbf{W}d\Omega_{2\mathrm{p}} + \rho_{\mathrm{c}}c_{\mathrm{Tc}}^2\int_{\Omega_{2\mathrm{c}}}\nabla\mathbf{W^T}\nabla\mathbf{W}d\Omega_{2\mathrm{c}} \tag{A38}$$

$$\mathbf{R}_2 = \rho_{\mathrm{p}}\omega^2\int_{\Omega_{2\mathrm{p}}}\mathbf{W^T}\mathbf{W}d\Omega_{2\mathrm{p}} + \rho_{\mathrm{c}}\omega^2\int_{\Omega_{2\mathrm{c}}}\mathbf{W^T}\mathbf{W}d\Omega_{2\mathrm{c}} \tag{A39}$$

$$\mathbf{Q}_{1x\pm} = ik\gamma^n\rho_{\mathrm{p}}c_{\mathrm{Tp}}^2\int_{\Gamma_{\mathrm{Ap}}}\mathbf{W^T}u_{1x\pm}^n d\Gamma_{\mathrm{Ap}}$$
$$+ ik\gamma^n\rho_{\mathrm{c}}c_{\mathrm{Tc}}^2\int_{\Gamma_{\mathrm{Ac}}}\mathbf{W^T}u_{1x\pm}^n d\Gamma_{\mathrm{Ac}} \quad n = 1,2\ldots m_1 \tag{A40}$$

$$\mathbf{Q}_{1zx\pm} = \rho_{\mathrm{p}}c_{\mathrm{Tp}}^2\int_{\Gamma_{\mathrm{Ap}}}\mathbf{W^T}\frac{\partial u_{1z\pm}^n}{\partial x}d\Gamma_{\mathrm{Ap}}$$
$$+ \rho_{\mathrm{c}}c_{\mathrm{Tc}}^2\int_{\Gamma_{\mathrm{Ac}}}\mathbf{W^T}\frac{\partial u_{1z\pm}^n}{\partial x}d\Gamma_{\mathrm{Ac}} \quad n = 1,2\ldots m_1 \tag{A41}$$

$$\mathbf{Q}_{3x+} = ik\gamma^n\rho_{\mathrm{p}}c_{\mathrm{Tp}}^2\int_{\Gamma_{\mathrm{Bp}}}\mathbf{W^T}u_{1x+}^n d\Gamma_{\mathrm{Bp}}$$
$$+ ik\gamma^n\rho_{\mathrm{c}}c_{\mathrm{Tc}}^2\int_{\Gamma_{\mathrm{Bc}}}\mathbf{W^T}u_{1x+}^n d\Gamma_{\mathrm{Bc}} \quad n = 1,2\ldots m_1 \tag{A42}$$

$$\mathbf{Q}_{3zx+} = \rho_{\mathrm{p}}c_{\mathrm{Tp}}^2\int_{\Gamma_{\mathrm{Bp}}}\mathbf{W^T}\frac{\partial u_{1z+}^n}{\partial x}d\Gamma_{\mathrm{Bp}} + \rho_{\mathrm{c}}c_{\mathrm{Tc}}^2\int_{\Gamma_{\mathrm{Bc}}}\mathbf{W^T}$$
$$\times \frac{\partial u_{1z+}^n}{\partial x}d\Gamma_{\mathrm{Bc}} \quad n$$
$$= 1,2\ldots m_1 \tag{A43}$$

$$\mathbf{Q}_{1y\pm} = ik\gamma^n\rho_{\mathrm{p}}c_{\mathrm{Tp}}^2\int_{\Gamma_{\mathrm{Ap}}}\mathbf{W^T}u_{1y\pm}^n d\Gamma_{\mathrm{Ap}}$$
$$+ ik\gamma^n\rho_{\mathrm{c}}c_{\mathrm{Tc}}^2\int_{\Gamma_{\mathrm{Ac}}}\mathbf{W^T}u_{1y\pm}^n d\Gamma_{\mathrm{Ac}} \quad n = 1,2\ldots m_1 \tag{A44}$$

$$\mathbf{Q}_{1zy\pm} = \rho_{\mathrm{p}}c_{\mathrm{Tp}}^2\int_{\Gamma_{\mathrm{Ap}}}\mathbf{W^T}\frac{\partial u_{1z\pm}^n}{\partial y}d\Gamma_{\mathrm{Ap}}$$
$$+ \rho_{\mathrm{c}}c_{\mathrm{Tc}}^2\int_{\Gamma_{\mathrm{Ac}}}\mathbf{W^T}\frac{\partial u_{1z\pm}^n}{\partial y}d\Gamma_{\mathrm{Ac}} \quad n = 1,2\ldots m_1 \tag{A45}$$

$$\mathbf{Q}_{3y+} = ik\gamma^n\rho_{\mathrm{p}}c_{\mathrm{Tp}}^2\int_{\Gamma_{\mathrm{Bp}}}\mathbf{W^T}u_{1y+}^n d\Gamma_{\mathrm{Bp}}$$
$$+ ik\gamma^n\rho_{\mathrm{c}}c_{\mathrm{Tc}}^2\int_{\Gamma_{\mathrm{Bc}}}\mathbf{W^T}u_{1y+}^n d\Gamma_{\mathrm{Bc}} \quad n = 1,2\ldots m_1 \tag{A46}$$

$$\mathbf{Q}_{3zy+} = \rho_{\mathrm{p}}c_{\mathrm{Tp}}^2\int_{\Gamma_{\mathrm{Bp}}}\mathbf{W^T}\frac{\partial u_{1z+}^n}{\partial y}d\Gamma_{\mathrm{Bp}}$$
$$+ \rho_{\mathrm{c}}c_{\mathrm{Tc}}^2\int_{\Gamma_{\mathrm{Bc}}}\mathbf{W^T}\frac{\partial u_{1z+}^n}{\partial y}d\Gamma_{\mathrm{Bc}} \quad n = 1,2\ldots m_1 \tag{A47}$$

$$\mathbf{Q}_{1z\pm} = ik\gamma^n\rho_{\mathrm{p}}c_{\mathrm{Lp}}^2\int_{\Gamma_{\mathrm{Ap}}}\mathbf{W^T}u_{1z\pm}^n d\Gamma_{\mathrm{Ap}}$$
$$+ ik\gamma^n\rho_{\mathrm{c}}c_{\mathrm{Lc}}^2\int_{\Gamma_{\mathrm{Ac}}}\mathbf{W^T}u_{1z\pm}^n d\Gamma_{\mathrm{Ac}} \quad n = 1,2\ldots m_1 \tag{A48}$$

$$\mathbf{Q}_{1xx\pm} = \rho_{\mathrm{p}}\left(c_{\mathrm{Lp}}^2 - 2c_{\mathrm{Tp}}^2\right)\int_{\Gamma_{\mathrm{Ap}}}\mathbf{W^T}\frac{\partial u_{1x\pm}^n}{\partial x}d\Gamma_{\mathrm{Ap}}$$
$$+ \rho_{\mathrm{c}}(c_{\mathrm{Lc}}^2 - 2c_{\mathrm{Tc}}^2)\int_{\Gamma_{\mathrm{Ac}}}\mathbf{W^T}\frac{\partial u_{1x\pm}^n}{\partial x}d\Gamma_{\mathrm{Ac}} \quad n = 1,2\ldots m_1 \tag{A49}$$

$$\mathbf{Q}_{1yy\pm} = \rho_{\mathrm{p}}\left(c_{\mathrm{Lp}}^2 - 2c_{\mathrm{Tp}}^2\right)\int_{\Gamma_{\mathrm{Ap}}}\mathbf{W^T}\frac{\partial u_{1y\pm}^n}{\partial y}d\Gamma_{\mathrm{Ap}}$$
$$+ \rho_{\mathrm{c}}(c_{\mathrm{Lc}}^2 - 2c_{\mathrm{Tc}}^2)\int_{\Gamma_{\mathrm{Ac}}}\mathbf{W^T}\frac{\partial u_{1y\pm}^n}{\partial y}d\Gamma_{\mathrm{Ac}} \quad n = 1,2\ldots m_1 \tag{A50}$$

$$\mathbf{Q}_{3z+} = ik\gamma^n\rho_{\mathrm{p}}c_{\mathrm{Lp}}^2\int_{\Gamma_{\mathrm{Bp}}}\mathbf{W^T}u_{1z+}^n d\Gamma_{\mathrm{Bp}}$$
$$+ ik\gamma^n\rho_{\mathrm{c}}c_{\mathrm{Lc}}^2\int_{\Gamma_{\mathrm{Bc}}}\mathbf{W^T}u_{1z+}^n d\Gamma_{\mathrm{Bc}} \quad n = 1,2\ldots m_1 \tag{A51}$$

$$\mathbf{Q}_{3xx+} = \rho_{\mathrm{p}}\left(c_{\mathrm{Lp}}^2 - 2c_{\mathrm{Tp}}^2\right)\int_{\Gamma_{\mathrm{Bp}}}\mathbf{W^T}\frac{\partial u_{1x+}^n}{\partial x}d\Gamma_{\mathrm{Bp}}$$
$$+ \rho_{\mathrm{c}}(c_{\mathrm{Lc}}^2 - 2c_{\mathrm{Tc}}^2)\int_{\Gamma_{\mathrm{Bc}}}\mathbf{W^T}\frac{\partial u_{1x+}^n}{\partial x}d\Gamma_{\mathrm{Bc}} \quad n = 1,2\ldots m_1 \tag{A52}$$

$$\mathbf{Q}_{3yy+} = \rho_{\mathrm{p}}\left(c_{\mathrm{Lp}}^2 - 2c_{\mathrm{Tp}}^2\right)\int_{\Gamma_{\mathrm{Bp}}}\mathbf{W^T}\frac{\partial u_{1y+}^n}{\partial y}d\Gamma_{\mathrm{Bp}}$$
$$+ \rho_{\mathrm{c}}(c_{\mathrm{Lc}}^2 - 2c_{\mathrm{Tc}}^2)\int_{\Gamma_{\mathrm{Bc}}}\mathbf{W^T}\frac{\partial u_{1y+}^n}{\partial y}d\Gamma_{\mathrm{Bc}} \quad n = 1,2\ldots m_1 \tag{A53}$$

$$\mathbf{M}_{1x\pm} = ik\gamma^m\rho_{\mathrm{p}}c_{\mathrm{Tp}}^2\int_{\Gamma_{\mathrm{Ap}}}u_{1x-}^m u_{1x\pm}^n d\Gamma_{\mathrm{Ap}}$$
$$+ ik\gamma^m\rho_{\mathrm{c}}c_{\mathrm{Tc}}^2\int_{\Gamma_{\mathrm{Ac}}}u_{1x-}^m u_{1x\pm}^n d\Gamma_{\mathrm{Ac}} \quad (m = 0,1,\ldots,m_1; n = 0,1,\ldots,m_1) \tag{A54}$$

$$\mathbf{M}_{1y\pm} = ik\gamma^m\rho_{\mathrm{p}}c_{\mathrm{Tp}}^2\int_{\Gamma_{\mathrm{Ap}}}u_{1y-}^m u_{1y\pm}^n d\Gamma_{\mathrm{Ap}}$$
$$+ ik\gamma^m\rho_{\mathrm{c}}c_{\mathrm{Tc}}^2\int_{\Gamma_{\mathrm{Ac}}}u_{1y-}^m u_{1y\pm}^n d\Gamma_{\mathrm{Ac}} \quad (m = 0,1,\ldots,m_1; n = 0,1,\ldots,m_1) \tag{A55}$$

$$\mathbf{M}_{1z\pm} = ik\gamma^m\rho_{\mathrm{p}}c_{\mathrm{Lp}}^2\int_{\Gamma_{\mathrm{Ap}}}u_{1z-}^m u_{1z\pm}^n d\Gamma_{\mathrm{Ap}} + ik\gamma^m\rho_{\mathrm{c}}c_{\mathrm{Lc}}^2$$
$$\times \int_{\Gamma_{\mathrm{Ac}}}u_{1z-}^m u_{1z\pm}^n d\Gamma_{\mathrm{Ac}} \quad (m = 0,1,\ldots,m_1; n = 0,1,\ldots,m_1) \tag{A56}$$

$$\mathbf{M}_{1zxx\pm} = \rho_{\mathrm{p}}c_{\mathrm{Tp}}^2\int_{\Gamma_{\mathrm{Ap}}}\frac{\partial u_{1z-}^m}{\partial x}u_{1x\pm}^n d\Gamma_{\mathrm{Ap}}$$
$$+ \rho_{\mathrm{c}}c_{\mathrm{Tc}}^2\int_{\Gamma_{\mathrm{Ac}}}\frac{\partial u_{1z-}^m}{\partial x}u_{1x\pm}^n d\Gamma_{\mathrm{Ac}} \quad (m = 0,1,\ldots,m_1; n = 0,1,\ldots,m_1) \tag{A57}$$

$$\mathbf{M}_{1zyy\pm} = \rho_{\mathrm{p}}c_{\mathrm{Tp}}^2\int_{\Gamma_{\mathrm{Ap}}}\frac{\partial u_{1z-}^m}{\partial y}u_{1y\pm}^n d\Gamma_{\mathrm{Ap}}$$
$$+ \rho_{\mathrm{c}}c_{\mathrm{Tc}}^2\int_{\Gamma_{\mathrm{Ac}}}\frac{\partial u_{1z-}^m}{\partial y}u_{1y\pm}^n d\Gamma_{\mathrm{Ac}} \quad (m = 0,1,\ldots,m_1; n = 0,1,\ldots,m_1) \tag{A58}$$

$$\mathbf{M}_{1xxz\pm} = \rho_p \left(c_{Lp}^2 - 2c_{Tp}^2 \right) \int_{\Gamma_{Ap}} \frac{\partial u_{1x-}^m}{\partial x} u_{1z\pm}^n d\Gamma_{Ap}$$
$$+ \rho_c \left(c_{Lc}^2 - 2c_{Tc}^2 \right) \int_{\Gamma_{Ac}} \frac{\partial u_{1x-}^m}{\partial x} u_{1z\pm}^n d\Gamma_{Ac} \quad (m = 0, 1, \dots, m_1; n = 0, 1, \dots, m_1)$$

(A59)

$$\mathbf{M}_{1yyz\pm} = \rho_p \left(c_{Lp}^2 - 2c_{Tp}^2 \right) \int_{\Gamma_{Ap}} \frac{\partial u_{1y-}^m}{\partial y} u_{1z\pm}^n d\Gamma_{Ap}$$
$$+ \rho_c \left(c_{Lc}^2 - 2c_{Tc}^2 \right) \int_{\Gamma_{Ac}} \frac{\partial u_{1y-}^m}{\partial y} u_{1z\pm}^n d\Gamma_{Ac} \quad (m = 0, 1, \dots, m_1; n = 0, 1, \dots, m_1)$$

(A60)

$$\mathbf{M}_{3x\pm} = ik\gamma^m \rho_p c_{Tp}^2 \int_{\Gamma_{Bp}} u_{1x+}^m u_{1x\pm}^n d\Gamma_{Bp}$$
$$+ ik\gamma^m \rho_c c_{Tc}^2 \int_{\Gamma_{Bc}} u_{1x+}^m u_{1x\pm}^n d\Gamma_{Bc} \quad (m = 0, 1, \dots, m_1; n = 0, 1, \dots, m_1)$$

(A61)

$$\mathbf{M}_{3y\pm} = ik\gamma^m \rho_p c_{Tp}^2 \int_{\Gamma_{Bp}} u_{1y+}^m u_{1y\pm}^n d\Gamma_{Bp}$$
$$+ ik\gamma^m \rho_c c_{Tc}^2 \int_{\Gamma_{Bc}} u_{1y+}^m u_{1y\pm}^n d\Gamma_{Bc} \quad (m = 0, 1, \dots, m_1; n = 0, 1, \dots, m_1)$$

(A62)

$$\mathbf{M}_{3z\pm} = ik\gamma^m \rho_p c_{Lp}^2 \int_{\Gamma_{Bp}} u_{1z+}^m u_{1z\pm}^n d\Gamma_{Bp}$$
$$+ ik\gamma^m \rho_c c_{Lc}^2 \int_{\Gamma_{Bc}} u_{1z+}^m u_{1z\pm}^n d\Gamma_{Bc} \quad (m = 0, 1, \dots, m_1; n = 0, 1, \dots, m_1)$$

(A63)

$$\mathbf{M}_{3zxx\pm} = \rho_p c_{Tp}^2 \int_{\Gamma_{Bp}} \frac{\partial u_{1z+}^m}{\partial x} u_{1x\pm}^n d\Gamma_{Bp}$$
$$+ \rho_c c_{Tc}^2 \int_{\Gamma_{Bc}} \frac{\partial u_{1z+}^m}{\partial x} u_{1x\pm}^n d\Gamma_{Bc} \quad (m = 0, 1, \dots, m_1; n = 0, 1, \dots, m_1)$$

(A64)

$$\mathbf{M}_{3zyy\pm} = \rho_p c_{Tp}^2 \int_{\Gamma_{Bp}} \frac{\partial u_{1z+}^m}{\partial y} u_{1y\pm}^n d\Gamma_{Bp}$$
$$+ \rho_c c_{Tc}^2 \int_{\Gamma_{Bc}} \frac{\partial u_{1z+}^m}{\partial y} u_{1y\pm}^n d\Gamma_{Bc} \quad (m = 0, 1, \dots, m_1; n = 0, 1, \dots, m_1)$$

(A65)

$$\mathbf{M}_{3xxz\pm} = \rho_p \left(c_{Lp}^2 - 2c_{Tp}^2 \right) \int_{\Gamma_{Bp}} \frac{\partial u_{1x+}^m}{\partial x} u_{1z\pm}^n d\Gamma_{Bp}$$
$$+ \rho_c \left(c_{Lc}^2 - 2c_{Tc}^2 \right) \int_{\Gamma_{Bc}} \frac{\partial u_{1x+}^m}{\partial x} u_{1z\pm}^n d\Gamma_{Bc} \quad (m = 0, 1, \dots, m_1; n = 0, 1, \dots, m_1)$$

(A66)

$$\mathbf{M}_{3yyz\pm} = \rho_p \left(c_{Lp}^2 - 2c_{Tp}^2 \right) \int_{\Gamma_{Bp}} \frac{\partial u_{1y+}^m}{\partial y} u_{1z\pm}^n d\Gamma_{Bp}$$
$$+ \rho_c \left(c_{Lc}^2 - 2c_{Tc}^2 \right) \int_{\Gamma_{Bc}} \frac{\partial u_{1y+}^m}{\partial y} u_{1z\pm}^n d\Gamma_{Bc} \quad (m = 0, 1, \dots, m_1; n = 0, 1, \dots, m_1)$$

(A67)

References

[1] J.J. Ditri, J.L. Rose, Excitation of guided elastic wave modes in hollow cylinders by applied surface tractions, J. Appl. Phys. 72 (7) (1992) 2589–2597.
[2] M.J.S. Lowe, D.N. Alleyne, P. Cawley, Defect detection in pipes using guided waves, Ultrasonics 36 (1998) 147–154.
[3] N. Barshinger, J.L. Rose, Guided wave propagation in an elastic hollow cylinder coated with a viscoelastic material, IEEE Trans. Ultrason. Ferroelectr. Freq. Control 51 (2004) 1547–1556.
[4] I. Bartoli, A. Marzani, F. Lanza di Scalea, E. Viola, Modeling wave propagation in damped waveguides of arbitrary cross-section, J. Sound Vib. 295 (2006) 685–707.
[5] T. Hayashi, W.-J. Song, J.L. Rose, Guided wave dispersion curves for a bar with an arbitrary cross-section, a rod and rail example, Ultrasonics 41 (2003) 175–183.
[6] S. Finnveden, Evaluation of modal density and group velocity by a finite element method, J. Sound Vib. 273 (2004) 51–75.
[7] V. Damljanović, R.L. Weaver, Propagating and evanescent elastic waves in cylindrical waveguides of arbitrary cross section, J. Acoust. Soc. Am. 115 (2004) 1572–1581.
[8] F. Treyssède, Elastic waves in helical waveguides, Wave Motion 121 (2008) 457–470.
[9] F. Treyssède, L. Laguerre, Numerical and analytical calculation of modal excitability for elastic wave generation in lossy waveguides, J. Acoust. Soc. Am. 133 (2013) 3827–3837.
[10] J. Mu, J.L. Rose, Guided wave propagation and mode differentiation in hollow cylinders with viscoelastic coatings, J. Acoust. Soc. Am. 124 (2008) 866–874.
[11] M. Castaings, M. Lowe, Finite element model for waves guided along solid systems of arbitrary section coupled to infinite solid media, J. Acoust. Soc. Am. 123 (2008) 696–708.
[12] A. Marzani, E. Viola, I. Bartoli, F. Lanza di Scalea, P. Rizzo, A semi-analytical finite element formulation for modelling stress wave propagation in axisymmetric damped waveguides, J. Sound Vib. 318 (2008) 488–505.
[13] A. Bernard, M.J.S. Lowe, M. Deschamps, Guided waves energy velocity in absorbing and non-absorbing plates, J. Acoust. Soc. Am. 110 (2001) 186–196.
[14] J. Hua, J.L. Rose, Guided wave inspection penetration power in viscoelastic coated pipes, Insight 52 (2010) 195–200.
[15] M.V. Predoi, M. Castaings, L. Moreau, Influence of material viscoelasticity on the scattering of guided waves by defects, J. Acoust. Soc. Am. 124 (5) (2008) 2883–2894.
[16] A. Żak, A novel formulation of a spectral plate element for wave propagation in isotopic structures, Finite Elem. Anal. Des. 45 (2009) 650–658.
[17] W. Ostachowicz, P. Kudela, M. Krawczuk, A. Żak, Guided Waves in Structures for SHM, John Wiley & Sons Ltd., U.K, 2012 (Chapter 2).
[18] J.M. Galán, R. Abascal, Remote characterization of defects in plates with viscoelastic coatings using guided waves, Ultrasonics 42 (2004) 877–882.
[19] W.J. Zhou, M.N. Ichchou, J.M. Mencik, Analysis of wave propagation in cylindrical pipes with local inhomogeneities, J. Sound Vib. 319 (2009) 335–354.
[20] F. Benmeddour, F. Treyssède, L. Laguerre, Numerical modelling of guided wave interaction with non-axisymmetric cracks in elastic cylinders, Int. J. Solids Struct. 48 (2011) 764–774.
[21] W. Duan, R. Kirby, A numerical model for the scattering of elastic waves from a non-axisymmetric defect in a pipe, Finite Elem. Anal. Des. 100 (2015) 28–40.
[22] R. Kirby, Z. Zlatev, P. Mudge, On the scattering of torsional elastic waves from axisymmetric defects in coated pipes, J. Sound Vib. 331 (2012) 3989–4004.
[23] R. Kirby, Z. Zlatev, P. Mudge, On the scattering of longitudinal elastic waves from axisymmetric defects in coated pipes, J. Sound Vib. 332 (2013) 5040–5058.
[24] B.A. Auld, Acoustic Fields in Waves and Solids, vol. 1, Krieger, Malabar, FL, 1990.